MOLECULAR INGREDIENTS OF HETEROGENEOUS CATALYSIS

CALIFORNIA UNIV., BERKELEY. LAWRENCE BERKELEY LAB

MAR 1984

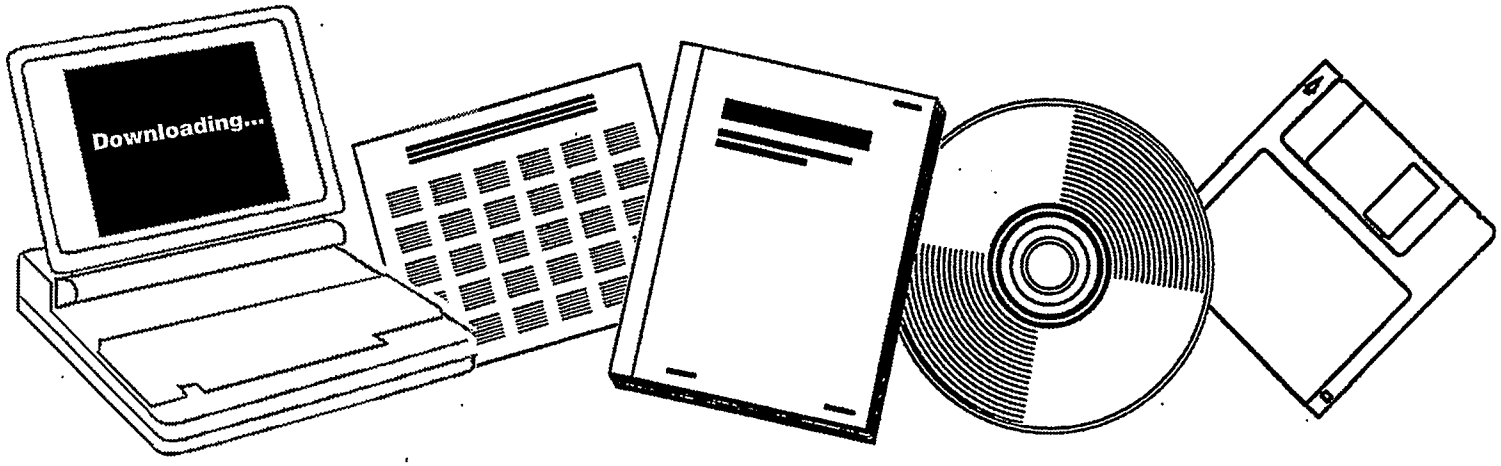

One Source. One Search. One Solution.

NTIS

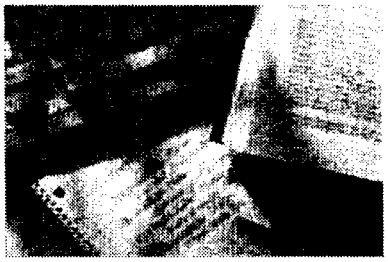

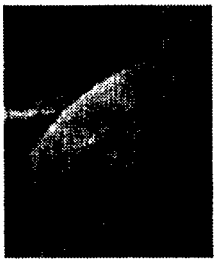

Providing Permanent, Easy Access to U.S. Government Information

National Technical Information Service is the nation's largest repository and disseminator of government-initiated scientific, technical, engineering, and related business information. The NTIS collection includes almost 3,000,000 information products in a variety of formats: electronic download, online access, CD-ROM, magnetic tape, diskette, multimedia, microfiche and paper.

Search the NTIS Database from 1990 forward

NTIS has upgraded its bibliographic database system and has made all entries since 1990 searchable on **www.ntis.gov.** You now have access to information on more than 600,000 government research information products from this web site.

Link to Full Text Documents at Government Web Sites

Because many Government agencies have their most recent reports available on their own web site, we have added links directly to these reports. When available, you will see a link on the right side of the bibliographic screen.

Download Publications (1997 - Present)

NTIS can now provides the full text of reports as downloadable PDF files. This means that when an agency stops maintaining a report on the web, NTIS will offer a downloadable version. There is a nominal fee for each download for most publications.

For more information visit our website:

www.ntis.gov

U.S. DEPARTMENT OF COMMERCE
Technology Administration
National Technical Information Service
Springfield, VA 22161

LBL-16983

MOLECULAR INGREDIENTS OF HETEROGENEOUS CATALYSIS

LBL--16983
DE84 010707

Presented at the Royal Society of Chemistry International Congress on Catalysis, London, England, November 7, 1983; and published in the Proceedings

By Gabor A. Somorjai

DISCLAIMER

Materials and Molecular Research Division,
Lawrence Berkeley Laboratory
and
Department of Chemistry,
University of California,
Berkeley, California 94720

Lecture was Delivered in November 1983

INTRODUCTION

When Professor Thomas asked me to join up with him for a symposium on catalysis, I was happy to oblige. Catalysis science stands on two legs, surface science and the solid state chemistry of metastable materials (Figure 1). In the last 10 years a scientific revolution occurred that converted catalysis from art to science. From the surface science side, this was due to atomic level characterization of model, low surface area and real, high surface area catalysts. As a result the preparation of catalysts and their application in the chemical and petrochemical technologies have become science driven. That is, the molecular level understanding that is obtained by research in the laboratory controls the development of chemical or petrochemical catalysis based technology. Two examples of recently developed high technology catalysts are the catalytic converter and the new generation of zeolites (Figures 2 and 3). These could not have been developed without the molecular level characterization of their structure and composition by electron spectroscopies and solid-state nmr that lead to the establishment of the all important correlation between their atomic structure and composition and performance.

Let me review this recent development of the molecular science of heterogeneous catalysis from the surface science side, where much of my research is concentrated, and perhaps also show the direction the field might take in the near future. My investigations utilize mostly small area single crystal catalysts and use the full repertoire of surface science techniques for their characterization. The most frequently used tools for surface characterization include low energy electron diffraction (LEED), Auger electron spectroscopy (AES), and high resolution electron energy loss spectroscopy (HREELS). The work horse for the catalytic studies was the low-pressure, high-pressure apparatus (2), shown in Figure 4. After appropriate characterization

the sample is enclosed in an isolation chamber that can be pressurized to atmospheric pressures (up to 100 atmosphere) with the reactant gases. These can be circulated by a pump and when the sample is heated to the reaction temperatures, the rate and the product distrubution can be monitored with a gas chromatograph. The high pressure loop acts as a microreactor that can be operated in the flow or in the batch modes. When the reaction is complete, the isolation cell is opened and the sample is now in an ultra-high vacuum environment again. After performing surface analysis to identify the surface composition and structure that was present under the reaction conditions, the surface may be modified and the high pressure reaction study can be continued.

When using model catalysts it is essential to establish if close similarity exists between the behavior of the model and the real catalyst systems. This was found to be the case for several reactions that include the hydrogenation of carbon monoxide over rhodium (3), the hydrogenation of cyclohexene (4) and the ring opening of cyclopropane (5).

We investigated, in some detail several important catalytic reactions. These include the conversion of hydrocarbons over Pt crystal surfaces (6,7,8), the synthesis of ammonia over iron (9) and rhenium (10) crystals, the hydrogenation of carbon monoxide over iron (11) and rhodium (12), and the photodissociation of water over TiO_2, $SrTiO_3$ (13) and iron oxides (14). From these studies three molecular ingredients of heterogeneous catalysis were identified. These are:

1. The Atomic Structure of the Surface
2. The Carbonaceous Deposit
3. The Oxidation State of Surface Atoms

We shall discuss each one of these ingredients and give examples of their roles in catalytic surface reactions.

1. Atomic Surface Structure: Figure 5 compares the rates of ammonia production on three single crystal surfaces of body centered cubic iron (9) at high pressures. The (111) face is about 430 times more active than the closest packed (110) crystal face while the (100) face is 32 times as active as the (110) face. The rate limiting step in this reaction is the dissociation of N_2 and it appears that this process occurs with a near zero activation energy on the (111) iron surface while there is a larger activation energy on the other iron crystal surfaces. It has been proposed that the active site for breaking the very strong N_2 bond is a seven coordinated iron atom that is present in the second layer under the surface. There is a theory being developed (15) that relates the concentration of nearly degenerate electron vacancy states, the density of hole states, near the Fermi level, to the ability of a given site to break and make chemical bonds in a transient manner by charge fluctuations. The sites with the largest number of nearest neighbors (highest coordination) have the highest density of electron-hole states and thus, they should be the most active during catalytic reactions. Unfortunately they are located in the bulk and are not accessible to the incoming reactants. However, atoms in the second layer of an open surface structure are accessible but are still surrounded by a large number of neighbors. These are then the most active sites in many catalytic reactions. While this theory will have to be tested further and proven by careful experiments, the available experimental data on the structure sensitivity of catalytic reactions can be explained

by it. Figure 6 shows the rate of ammonia formation from N_2 and H_2 over hexagonal close packed rhenium crystal surfaces (16). Again the open $(11\bar{2}0)$ crystal face is about a 10^3 times more active than the closest packed (0001) hexagonal surface, thus exhibiting a profound structure sensitivity that is even more pronounced as that on iron.

For catalyzed hydrocarbon reactions on platinum that is an excellent catalyst there are four crystal surfaces with very different atomic surface structures that exhibit very different reaction selectivities. These are the flat (111) and (100) surfaces that have hexagonal and square unit cells, respectively. The other two surfaces have ordered steps of atomic heights and one has ledges (or kinks) in the steps as well. These are shown in Figure 7. The test reactions that best demonstrate the structure sensitivity over Pt is the conversion of n-hexane and n-heptane to other organic molecules (6). N-hexane may convert to benzene upon dehydrocyclization or to methycyclopentane by a cyclization reaction. These are shown in Figure 8. It may isomerize to branched butanes or undergo C-C bond breaking (hydrogenolysis) to produce C_1-C_3 fragments (methane to propane). The first three of these reactions are desirable when the aim is to produce high octane gasoline while the fourth reaction is undesirable as it leads to the production of gases of much less value as fuels. Figure 9 shows that the hexagonal surface produces much more aromatic products than the square (100) crystal face. In fact, a stepped surface with (111) orientation terraces that are 5 atoms wide is perhaps the best catalyst we found so far to carry out the dehydrocyclization reaction. Conversely, the (100) flat surfaces with the square unit cells are much better isomerization catalysts, as shown in Figure 10,

than the hexagonal crystal surface of Pt (7). Thus, depending on the catalyst preparation, one may obtain superior dehydrocyclization or isomerization activity that is certainly well documented in the patent literature. The hydrogenolysis reaction that is also shown in Figure 10 is most active on surfaces that contain a large concentration of ledge or kink sites (8). It is often necessary to "poison" these sites by the adsorption of sulfur or other strongly bound additives that bind more strongly to the ledge sites than to the other surface sites (step or terrace sites). This way, the ledges cannot participate in hydrocarbon reactions because they are masked by the selective adsorption of additives while the rest of the higher coordination surface sites remain clean and thereby active and selective.

2. The Carbonaceous Deposit:

A catalytically active metal surface is always covered with a carbonaceous deposit. By labeling the reactant organic molecules with ^{14}C isotope, the residence time of this carbonaceous layer can be monitored (17). It is found that it is usually ten to fifty times larger than the turnover time for the catalytic hydrocarbon conversion reactions. This is shown in Figure 11 under the label of irreversible adsorption along with the hydrogen to carbon ratio of this deposit. As the reaction temperature is increased, the deposit becomes successively dehydrogenated as its stoichiometry varies from C_2H_3 to C_2H and finely it looses all its hydrogen, and becomes graphitic. While the metal surface retains its catalytic activity as long as the carbonaceous deposit contains hydrogen it becomes completely inactive, poisoned in the presence of the graphitic overlayer.

The sequential dehydrogenation of adsorbed organic monolayers with increasing temperature can be readily demonstrated by temperature programmed thermal desorption studies. Figure 12 shows the evolution of hydrogen from adsorbed layers of C_2H_4, C_3H_6, and C_4H_8 (18). At well defined temperatures, hydrogen evolves at a maximum rate until complete dehydrogenation and graphitization of the remaining carbon occurs at the highest temperatures.

LEED and HREELS studies reveal the structure of organic monolayers at each stage of chemisorption. At lower temperatures (<~300K) the organic molecules exhibit ordered molecular structures. Figure 13 shows one of the ordered surface structures of benzene (19) on the Rh(111) crystal face that was determined by LEED and Figure 14 shows the HREELS spectra of benzene and its deuterated form (20). The C_{3v} symmetry is clearly compatible with the molecular structure shown in Figure 13 with the molecule lying with its π ring parallel to the surface and the center of the ring above a three-fold hollow. Figure 15 shows the surface structures of chemisorbed ethylene, propylene and butene on the Pt(111) crystal face (21). These molecules form alkylidyne species upon adsorption near 300K with their C-C bond, that is closest to the metal surface, perpendicular and elongated to a single C-C bond length. Similar alkylidyne structures have been found on other transition metal surface, as well that include Pd, Rh and Ni (22). The carbon atom that binds the molecule to the metal prefers the 3-fold hollow site. Figure 16 compares the molecular structure of the ethylidyne molecule on the Pt(111) surface with a structure of ethylidyne containing trinuclear metal cluster compounds. The symmetry, the bond distances and bond angles in these clusters are very similar to the molecular structure

of chemisorbed ethylene on the transition metal surface. This similarity indicates the predominance of localized bonding of adsorbed surface species, an important conclusion in our scrutiny of the surface chemical bond (23).

Figure 17 shows the sequential change of the vibrational spectrum of chemisorbed C_2H_4 on the Rh(111) crystal face as the temperature is increased (24). The molecule decomposes and there is evidence for the presence of CH,C_2 and C_2H species on the surface in the spectra. Figure 18 shows schematically many of these species that were detectable by HREELS (not by LEED because these fragments are disordered) and also $-CH_3$ that has not been observed as yet (25). It is believed that the location of these organic fragments is governed by the necessity of tetrahedral symmetry for the bonding carbon atoms. That is a ≡CH fragment occupies a 3-fold site with bonding to 3 metal atoms; a CH_2 fragment has two metal bonds at a bridge site and by analogy a $-CH_3$ fragment should have one metal bond and be localized at a top site. If this is the desired bonding configuration of the various fragments, it explains the mechanism by which the 3-fold strongly binding sites are freed up by successive hydrogenation of the fragments and becomes available to the next incident molecule.

The alkylidyne molecules are present only under conditions of catalyzed reactions at low temperatures, as they decompose above 400K on most transition metal surfaces. This restricts their importance by and large to hydrogenation reactions which having low activation energies may proceed well below 400K. Recent studies of C_2H_4 hydrogenation over

Pt and Rh(111) crystal faces indicate that it occurs on top of the ethylidyne layer that remains ordered and its residence times is much longer than the turnover time of C_2H_4 hydrogenation (26).

For other catalyzed hydrocarbon reactions that occur at an appreciable rate only at higher temperatures the organic fragments are the permanent fixture on the surface during the reaction. Their main role appears to be H-transfer to the adsorbed reaction intermediates as the C-H bonds retain the hydrogen more easily than the bare transition metal surface. H-D exchange studies using pre-deuterated fragments or reactants indicate that the rate of H-D exchange is at least an order of magnitude faster than the turnover rate of most hydrocarbon conversion reactions. Thus, the hydrogen atoms in the C-H bonds of the strongly held organic fragments are readily transferred to the adsorbed intermediates while the carbon atom does not exchange easily.

Fortunately not all of the metal sites are covered with the organic fragments although AES studies indicate that more than a monolayer of carbon present on the surface under catalytic reaction conditions. We can titrate the remaining bare metal sites by the chemisorption of CO at low pressures which, under the same conditions, does not adsorb on the carbonaceous deposit (6). Figure 19 shows the fraction of the bare metal surface $(\theta/\theta_0)_{CO}$ that is present after the reaction where θ_0 is the concentration of chemisorbed CO on the initially clean metal surface before the reaction. About 5 - 20% of the Pt is uncovered, the bare metal area decreasing with increasing reaction temperatures. Of course at higher

hydrogen pressures (all hydrocarbon conversion reactions are carried out in the presence of excess hydrogen) the fraction of uncovered metal increases.

From these studies a molecular model of the working Pt catalyst can be constructed and is shown in Figure 20. There are bare metal islands whose structure is determined mostly by the catalyst fabrication (6). The incident reactant molecules adsorb and undergo chemical rearrangements on these metal islands. Then the adsorbed intermediates diffuse onto the carbonaceous deposit, pick up one or more hydrogen, and desorb as the products. Once the carbon deposit lost all its hydrogen and becomes graphitic hydrogen transfer that is an important part of the catalytic reactions can no longer occur and the catalyst surface becomes inactive.

3. Oxidation State of Surface Atoms:

The importance of different oxidation states of transition metal ions can well be demonstrated through the studies of the CO/H_2 reaction over rhodium (12). The metal produces mostly methane as shown in Figure 21, because it dissociates CO and has superior hydrogenating ability. However, over Rh_2O_3 surfaces a large fraction of oxygenated molecules CH_3CHO, CH_3OH and C_2H_5OH form. When the rhodium ion is incorporated into the crystal lattice of a refractory oxide such as La_2O_3 in the form of $LaRh_2O_3$ the products of the CO/H_2 reaction are exclusively oxygenated hydrocarbons (27). This drastic change in reaction selectivity has several causes. Figure 22 shows the heats of adsorption of CO and D_2 on the rhodium metal, Rh_2O_3 and $LaRhO_3$ surfaces. Rh_2O_3 binds CO more weakly and D_2 more strongly than the rhodium metal. However, the active $LaRhO_3$ appears to have at least

two binding states indicating that the transition metal is present on the active surface in at least two different oxidation states.

Rhodium-oxide has a unique ability to carbonylate olefins, an important step toward the formation of oxygenated species. When C_2H_4 is added to the CO/H_2 reactant mixture it is carbonylated quantitatively to propionaldehyde. On rhodium metal, ethylene was hydrogenated fully to ethane. Thus, oxidation of the metal reduces its hydrogenation ability and makes it active for carbonylation.

The difficulty is to maintain the higher metal oxidation states that produce desireable products under conditions of the catalytic reactions that occur in a highly reducing atmosphere. The refractory oxide support plays a key role in this circumstance. The Auger spectra of Rh_2O_3 before and after the CO/H_2 reaction indicates that the oxide is reduced to the metal within an hour with the corresponding change of the product distribution from the oxygenated species to methane. However, $LaRhO_3$ does not loose its lattice oxygen and the Rh^{3+} ion is fixed in the crystal lattice by the large lattice energy. Thus, the higher oxidation state transition metal ion is kinetically stabilized in the reducing reaction mixture and remains stable indefinitely as long as the temperature is not increased too high. The so-called strong metal support-interaction is often used to stabilize one or more different oxidation states of transition metal ions. Thus, the catalyst support plays an important chemical role in most catalyst systems in addition to providing high surface areas on which the metal component may be finely dispersed.

Another example of the importance of the changing oxidation state of transition metal ions at the surface is shown by the catalytic cycle leading to the photocatalyzed dissociation of H_2O or $SrTiO_3$ surfaces (28). This is shown in Figure 23. The oxide surface is completely hydroxylated in the presence of water and the Ti ion are in the 4+ formal oxidation state. When the surface region is irradiated with light of 3.1 eV or larger energy electron-hole pairs are generated. The electron is utilized to reduce the Ti^{4+} to the Ti^{3+} formal oxidation state. The electron vacancy induces charge transfer from the hydroxyl group that produces OH radicals that dimerize to H_2O_2 and splits off oxygen that evolves (29). The reduced Ti^{3+} containing surface can now adsorb another water molecule that acts as an oxidizing agent to produce Ti^{4+} again and a hydroxilated surface evolving hydrogen in the process. Clearly changes of oxidation states of transition metal ions are frequently indispensable reaction steps in catalytic processes.

4. The Building of Catalysts

By giving the examples of surface and catalytic studies on well characterized systems I hoped to demonstrate the understanding that could be achieved of the molecular ingredients of important catalytic systems. We can now utilize this understanding to build better systems by alteration of their structure or their state of surface charge. Below we discuss two examples of deliberate catalyst modifications: the effects of gold on transition-metal catalysis and the effects of potassium.

4a. The Effect of Gold on the Selectivity and Activity of Pt Catalysts

The influence of gold on Pt hydrocarbon conversion catalysis has been studied by condensing Au on Pt crystal surfaces. Gold forms epitaxial layers on Pt and upon heating it forms an alloy in the near surface region (30). This Au-Pt alloy has a markedly different selectivity and activity for the conversion of n-hexane to other hydrocarbons as shown in Figure 24. The isomerization rate goes up as compared to that on clean Pt while the hydrogenolysis and dehydrocyclization rates are reduced exponentially with increasing gold concentration (31). This remarkable selectivity and activity alteration can be explained by a change of structure of the Pt(111) surface induced by gold alloying. By substitution of a gold atom the high coordination 3-fold Pt sites are eliminated much faster than the two fold and one fold bridge and top sites. This is commonly called the ensemble effect. As a result, the chemistry that requires the adsorption of molecules and surface intermediates at the 3-fold sites is eliminated while the chemical reactions that require adsorption at bridge or top sites are not attenuated. While subtle electronic changes may also occur at the alloy surface sites, most of the results can be rationalized by this selective high coordination site elimination model.

Similar observations were reported by Boudart et al for the production of water from H_2 and O_2 over Pd-Au alloy surfaces. Small amounts of gold increased the rate of this reaction by fifty fold.

It should be noted that gold is a very poor catalyst for both of these reactions. Nevertheless, its presence as an alloying constituent can beneficially influence the selectivity and the reactivity of transition metal catalysts.

4b. The Effect of Potassium on the Bonding and Reactivity of Carbon Monoxide and Hydrocarbons

Potassium has a high heat of adsorption when present in low coverages on transition metal surfaces (Figure 25). Simultaneously it also reduces the work function of the transition metals indicating large charge transfer between the metals (32). A model that assumes that potassium is ionized when adsorbed on the transition metal surface explains these results. As the potassium concentration increases the charged species repell each other and depolarization occurs; the potassium layer becomes metallic and its heat of adsorption approaches rapidly the heat of sublimation of potassium metal.

Potassium has a strong influence on the heat of adsorption of CO on transition metal surfaces. This is shown in Figure 26. In the absence of potassium, CO desorbs at a maximum rate from the Rh(111) surface at 400K. However, when co-adsorbed with 50% of a monolayer of potassium, it desorbs at 600K indicating a 12 kcal increase of its binding energy (33). The HREELS spectra of CO on Pt(111) also exhibits major changes that are shown in Figure 27. In the absence of CO two well defined CO stretching frequencies are detectable that are associated with CO at a top and at a bridge site adsorbed with its CO bond perpendicular to the surface (33). As the potassium is added to the Rh surface CO shifts to the bridge site and its stretching frequency decreases by more than 300 cm^{-1} (34). This corresponds

to a gradual change of bond order with increasing potassium coverage from 2 to 1.5. This indicates that the electron transferred from the potassium to the transition metal density of states can populate the antibonding molecular orbitals of CO, thereby weakening the C-O bond. Simultaneously the metal carbon bond is strengthened as charge density in this bonding orbital must increase.

Potassium is often used as a beneficial additive to transition metal catalysts utilized for the hydrogenation of carbon monoxide. Its presence increases the molecular weight of hydrocarbon products as expected if the dissociation rate of carbon monoxide is enhanced.

Potassium however is a non-selective poison for hydrocarbon reactions on platinum surfaces (35). The reason for this is revealed in recent surface studies. The presence of potassium increases the activation energy for the breaking of C-H bonds that is an important step in most hydrocarbon conversion reactions. This is shown in Figure 28. Thus, the surface residence time of the molecules increase that reduces the catalytic turnover rates.

There is little doubt that potassium influences the catalytic reaction by charge transfer, that is, by electronic changes. It has large effects on some molecules when coadsorbed with them (CO, N_2) and virtually no effects on others (NO, PF_3) (36). It would be of value if we could predict by the use of theoretical guidance whether charge transfer between the molecular orbitals of adsorbates and the charge density that is altered by the adsorption of potassium on the transition metal surface could or could not take place.

5. New Reactions, New Processes

As our understanding of how catalysts work increases through the application of molecular surface science, it will be increasingly possible to find catalysts for reactions for which good catalysts do not seem to exist. There are many important reactions of small molecules that include CO_2, CH_4, H_2O and N_2 that may be investigated. CO_2 could be well utilized as a source of carbon containing chemicals if it is hydrogenated to HCOOH or dissociated to CO. Figure 29 shows the free energy changes associated with several reactions. While CO_2 hydrogenation is thermodynamically feasible, its dissociation to CO and O_2 requires the input of excess energy in the form of light or heat. The reaction of carbon with water to produce CH_4 and CO_2 is thermoneutral, as shown in Figure 29. This reaction may represent a desirable alternative for carbon gasification with water to CO and H_2, a very exothermic reaction indeed.

The partial oxidation of methane to CH_2O and CH_3OH should be feasible by suitable catalyst surfaces (37). These reactions are shown in Figure 29c. Finally, the oxidation of nitrogen to nitric acid ($N_2O + 5/2\ O_2 + H_2O \rightarrow 2H^+ + 2NO_3^-$) is thermodynamically feasible as pointed out by G. N. Lewis in 1923 (38).

"Even when starting with water and air, we see by our equations that nitric acid should form until it reaches a concentration of about 0.1M where the calculated equilibrium exists. It is to be hoped that nature will not discover a catalyst for this reaction, which would permit all of the oxygen and part of the nitrogen of the air to turn the oceans into dilute nitric acid."[1]

1. G.N. Lewis: Thermodynamics, page 568 (1923).

ACKNOWLEDGEMENTS

This work was supported by the Director, Office of Energy Research, Office of Basic Energy Sciences, Materials and Chemical Sciences Division of the U. S. Department of Energy under Contract Number DE-AC03-76SF00098.

FIGURE CAPTIONS

Figure 1: Schematic representation of the close relationship between the materials chemistry of metastable high surface area materials, surface science, and catalysis science.

Figure 2: The catalytic converter for the complete combustion of automobile exhaust. It oxidizes unburned hydrocarbons, and carbon monoxide to carbon dioxide and water, and reduces nitrogen oxides to dinitrogen simultaneously.

Figure 3: Two recently synthesized zeolites with large silicon to aluminum ratios.

Figure 4: Schematic representation of the experimental apparatus utilized to carry out the catalytic reaction rate studies on single crystal or polycrystalline surfaces of low surface area at low and high pressures in the 10^{-7} to 10^{+4} torr range.

Figure 5: The remarkable surface structure sensitivity of the iron catalyzed ammonia synthesis.

Figure 6: The structure sensitivity of ammonia synthesis on rhenium single crystal surfaces.

Figure 7: Idealized atomic surface structures for the flat platinum (111) and platinum (100), the stepped platinum (775) and kinked platinum (10,8,7) surfaces.

Figure 8: Skeletal rearrangement reactions of hydrocarbons catalyzed by platinum with high activity and unique selectivity. Depicted here are the several reaction pathways which occur simultaneously during the catalyzed conversion of n-hexane, C_6H_{14}. The isomerization, cyclization and aromatization reactions that produced branched or cyclic products are important in the production of high octane gasoline from petroleum naphtha. The hydrogenolysis reaction that involves breaking of C-C bonds yields undesirable gaseous products.

Figure 9: Dehydrocyclization of alkanes to aromatic hydrocarbons is one of the most important petroleum reforming reactions. The bar graphs shown here compare reaction rates for n-hexane and n-heptane aromatization catalyzed at 573 K, and atmospheric pressures over the two flat platinum single crystal faces with different atomic structure. The platinum surface with the hexagonal atomic arrangement is several times more active than the surface with a square unit cell over a wide range of reaction conditions.

Figure 10: Reaction rates are shown as a function of surface structure for isobutane isomerization and hydrogenolysis catalyzed at 570 K at atmospheric pressure over four platinum surfaces. The rates for both reaction pathways are very sensitive to structural features of the model single crystal catalytic surfaces. Isomerization of these light alkanes favored on the platinum surfaces that have a square (100) atomic arrangement

Figure 10: (continued) Hydrogenolysis rates are maximized when kinked sites are present at high concentrations as in the platinum (10,8,7) crystal surface.

Figure 11: Carbon 14 labeled ethylene C_2H_4 was chemisorbed as a function of temperature on a flat platinum surface with hexagonal orientation, Pt(111). H/C composition of the adsorbed species was determined from hydrogen thermal desorption studies. The amount of preadsorbed ethylene, which could not be removed by subsequent treatment in 1 atmosphere of hydrogen represents the irreversibly adsorbed fraction. The adsorption reversibility decreases markedly with increasing adsorption temperature as the surface species becomes more hydrogen deficient. The irreversibly adsorbed species have very long surface residence times on the order of days.

Figure 12: Hydrogen thermal desorption spectra illustrating the sequential dehydrogenation of ethylene, propylene, and cis-2-butene chemisorbed on Pt(111) at about 120K (the heating rate is 12 K per second).

Figure 13: The surface structure of benzene as determined from low energy diffraction studies and surface crystallography.

Figure 14: The vibrational spectra of benzene and deuterated benzene as determined by high resolution electron energy loss spectroscopy.

Figure 15: Surface structures for alkylidyne species formed on platinum (111) after the adsorption and rearrangement of ethylene, propylene and butenes. These structures were determined by LEED surface crystallography.

Figure 16: The surface structure of ethylidyne, the bond distances and angles, are compared with several tri-nuclear metal cluster compounds of similar structure.

Figure 17: Changes of the vibrational spectrum of chemisorbed ethylene as a function of increasing temperature. Sequential decomposition is clearly visible from the vibrational spectrum obtained by high resolution electron energy loss spectroscopy.

Figure 18: Schematic representation of the various organic fragments that are present on metal surfaces at higher temperature. The presence of CH, C_2, C_2H, CH_2 and $C-CH_3$ species have been detected.

Figure 19: Fractional concentrations of uncovered platinum surface sites determined by CO adsorption desorption as a function of surface carbon coverage on the (100), (111), and (13,1,1) platinum crystal surfaces. A comparison is made between the CO uptake determined following n-hexane reaction studies and CO uptake determined when CO was coadsorbed with graphitic surface carbon.

Figure 20: Model for the working platinum catalyst that was developed from our combination of surface studies using single crystal surfaces and hydrocarbon reaction rate studies on these same surfaces.

Figure 21: Product distribution in the carbon monoxide hydrogenation reaction on various rhodium compound surfaces.

Figure 22: Heat of desorption (kcal/mole) of CO and D_2 from lanthanum oxide, fresh and used lanthanum rhodate, fresh and used rhodium oxide and rhodium metal. The spread of each value represents the variation with surface coverage rather than experimental uncertainty.

Figure 23: A proposed mechanism for the photodissociation of water over TiO_2 and $SrTiO_3$ surfaces.

Figure 24: The rate of formation of various products from n-hexane as a function of fractional gold surface coverage for gold platinum alloys that were prepared by vaporizing and diffusing gold into Pt(111) crystal surfaces.

Figure 25: The heat of adsorption of potassium on platinum single crystal surfaces as a function of potassium coverage.

Figure 26: CO thermal desorption spectrum from clean platinum and when coadsorbed with potassium on platinum crystal surfaces.

Figure 27: Vibrational spectra of CO at the saturation coverage when chemisorbed on Pt(111) at 300 K as a function of preadsorbed potassium coverage.

Figure 28: Activation energy of the hydrogen β-elimination from carbonaceous deposits after n-hexane reactions over platinum (111) surfaces as a function of potassium coverages.

Figure 29 (a),(b) and (c): Standard free energies for several chemical reactions.

REFERENCES

1. G.A. Somorjai, Chemistry in Two Dimensions: Surfaces, Cornell University Press, (1981). Library of Congress Catalog Card No. 80-21443.

2. A.L. Cabrera, N.D. Spencer, E. Kozak, P.W. Davies and G.A. Somorjai, Rev. Sci. Instru. 53(12) (1982) 1888-1893.

3. B.A. Sexton and G.A. Somorjai, J. Catal. 46 (1977) 167.

4. S.M. Davis and G.A. Somorjai, J. Catal. 65 (1980) 78.

5. D.R. Kahn , E.E. Petersen and G.A. Somorjai, J. Catal. 34 (1974) 294.

6. W.D. Gillespie, R.K. Herz, E.E. Petersen and G.A. Somorjai, J. Catal. 70 (1981) 147.

7. S.M. Davis, F. Zaera and G.A. Somorjai, J. Am. Chem. Soc., 104 (1982) 7453-7461.

8. S. Mark Davis, F. Zaera and G.A. Somorjai, J. Catal. 85(1) (1984) 206.

9. N.D. Spencer, R.C. Schoonmaker and G.A. Somorjai, J. Catal. 74 (1982) 129.

10. N.D. Spencer and G.A. Somorjai, J. Catal. 78 (1982) 142-146.

11. D. Dwyer and G.A. Somorjai, J. Catal. 56 (1979) 249.

12. D.G. Castner, R.L. Blackadar and G.A. Somorjai, J. Catal. 66 (1980) 257.

13. F.T. Wagner and G.A. Somorjai, J. Am. Chem. Soc. 102 (1980) 5494.

14. C. Leygraf, M. Hendewerk and G.A. Somorjai, J. Catal., 78 (1982) 341-351.

15. L. Falicov and G.A. Somorjai, Proc. Natl. Acad. of Sci., to be published (1984).

16. M. Asscher and G.A. Somorjai, Surf. Sci., in press (1984).

17. S.M. Davis, F. Zaera and G.A. Somorjai, J. Catal. 77 (1982) 439-459.

18. M. Salmeron and G.A. Somorjai, J. Phys. Chem. 86 (1982) 341.

19. M.A. Van Hove, R. .in and G.A. Somorjai, Phys. Rev. Letters 51(9) (1983) 778-781.

20. B.E. Koel, J.E. Crowell, C.M. Mate and G.A. Somorjai, J. Phys. Chem., in press (1984).

21. R.J. Koestner, J.C. Frost, P.C. Stair, M.A. Van Hove and G.A. Somorjai, Surf. Sci. 116 (1982) 85-103.

22. R.J. Koestner, M.A. Van Hove and G.A. Somorjai, Surf. Sci., 121 (1982), 321-337.

23. G.A. Somorjai, Proc. 9th Intl. Conf. on Atomic Spectroscopy, XXII CSI, Tokyo, June 1982, Recent Advances in Analytical Spectroscopy, ed. K. Fuwa, Pub. Pergamon Press, (1982) 211.

24. B.E. Koel, J.E. Crowell, C.M. Mate and G.A. Somorjai, J. Phys. Chem., submitted for publication (1984).

25. C. Minot, M.A. Van Hove and G.A. Somorjai, Surf. Sci., 127 (1982) 441-460.

26. F. Zaera and G.A. Somorjai, J. Am. Chem. Soc., in press (1983).

27. P.R. Watson and G.A. Somorjai, J. Catal. 74 (1982) 282-295.

28. F.T. Wagner, S. Ferrer and G.A. Somorjai, in Photoeffects at Semiconductor-Electrolyte Interfaces, ed. A.J. Nozik, ACS Symposium Series 146, Washington, (1981).

29. Van Damme and K. Hall, J. Am. Chem. Soc. 101 (1980) 4373.

30. J.W.A. Sachtler, M.A. Van Hove, J.P. Biberian and G.A. Somorjai, Surf. Sci. 110 (1981) 19.

31. J.W.A. Sachtler and G.A. Somorjai, J. Catal., 81 (1983) 77-94.

32. E.L. Garfunkel and G.A. Somorjai, Surf. Sci. 115 (1982) 441.

33. E.L. Garfunkel, J.E. Crowell and G.A. Somorjai, J. Phys. Chem. 86 (1982) 310.

34. J.E. Crowell and G.A. Somorjai, Summary Abstract for the American Vacuum Society 30th National Vacuum Symposium, Nov. 1-4, 1983, Boston, Massachusetts, J. Vac. Sci. Tech., submitted for publication (1983).

35. F. Zaera and G.A. Somorjai, J. Catal., 84(2) (1983) 375.

36. E.L. Garfunkel, J.J. Maj, J.C. Frost, M.H. Farias and G.A. Somorjai, J. Phys. Chem., 87(19) (1983) 3629.

37. M.M. Khan and G.A. Somorjai, J. Catal., to be published (1984).

38. Thermodynamics, G.N. Lewis and N. Randall, McGraw Hill (1923).

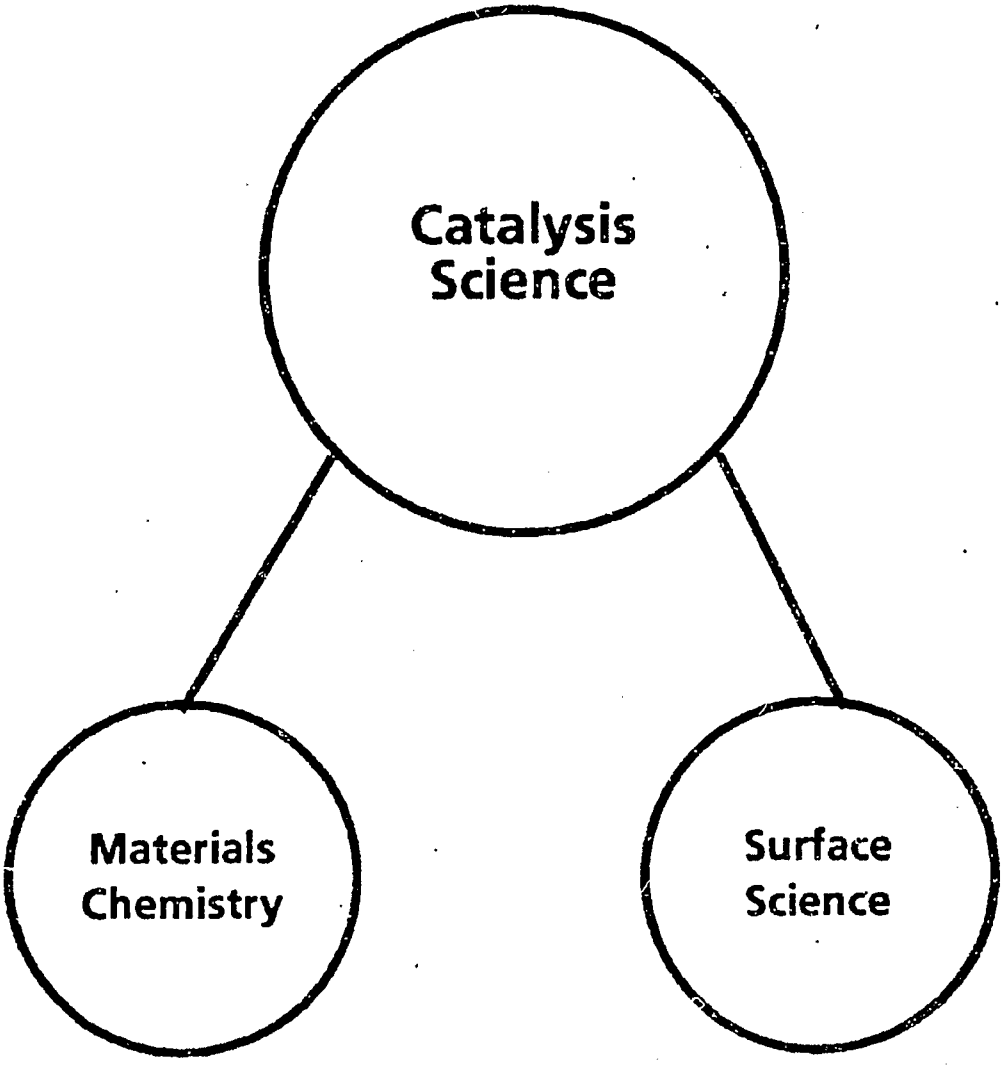

XBL 843-941

Fig.1

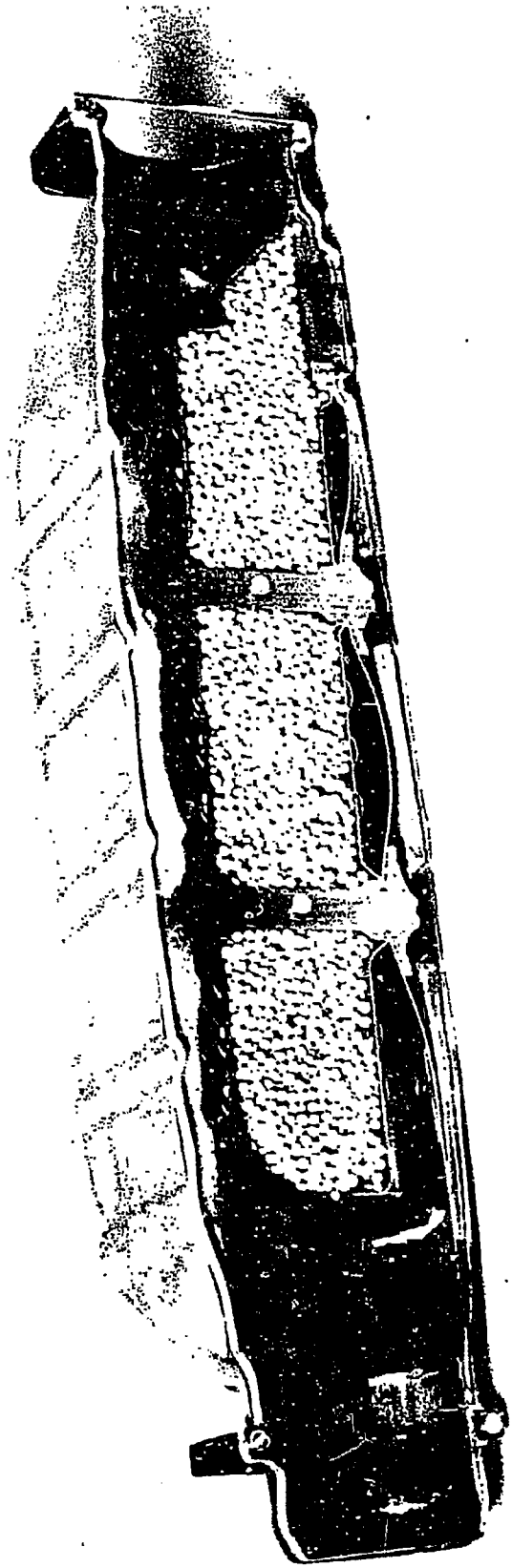

CBB 843-1518

FIG. 2

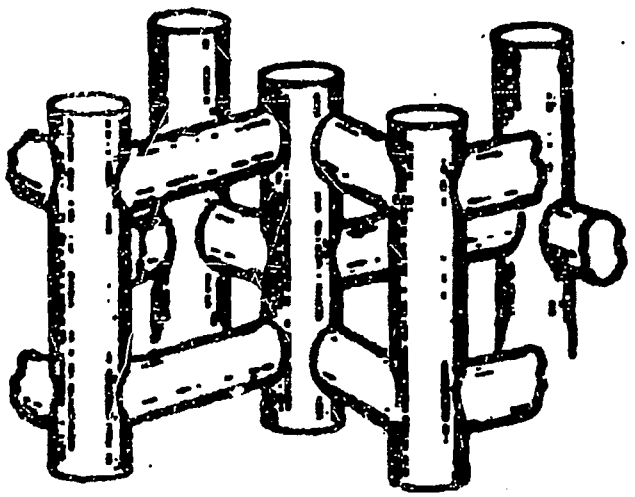

ZSM-5 Channel Structure

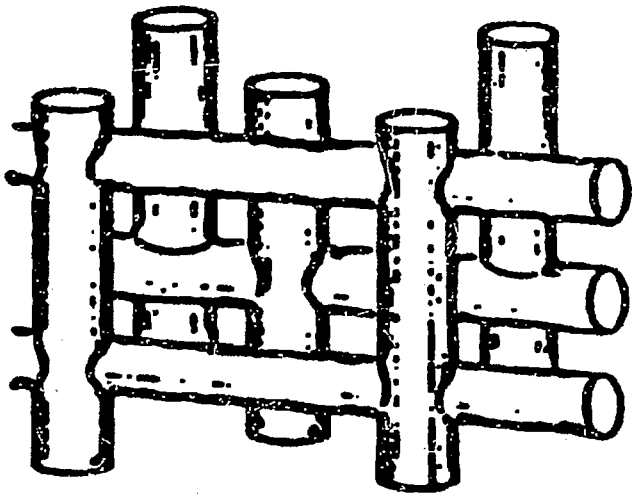

ZSM-11 Channel Structure

XBL 8310-12074

Fig. 3

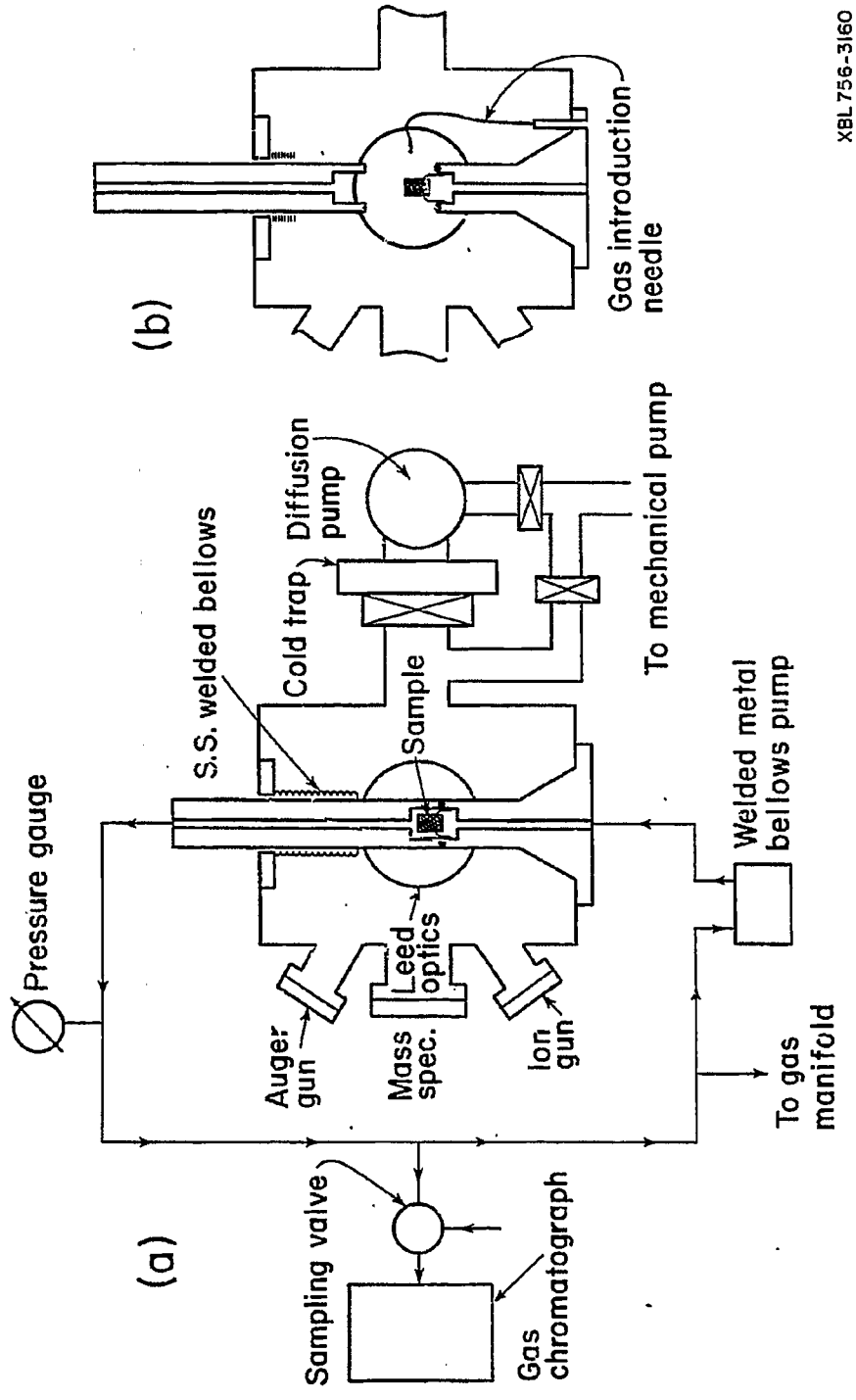

XBL 756-3160

Fig. 4

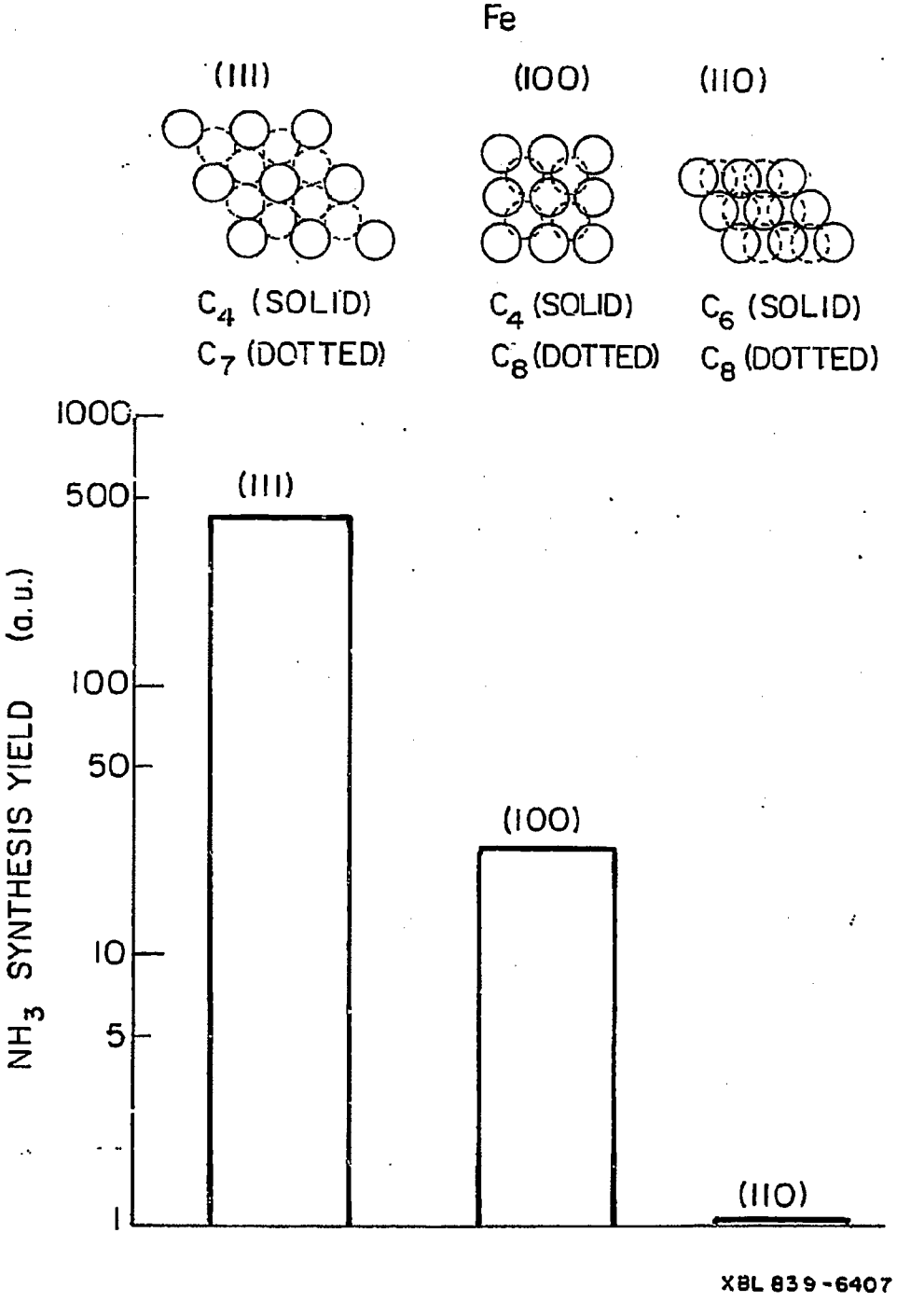
Fe
(111)
(100)
(110)
C_4 (SOLID)
C_7 (DOTTED)
C_4 (SOLID)
C_8 (DOTTED)
C_6 (SOLID)
C_8 (DOTTED)
1000
500
100
50
10
5
1
NH_3 SYNTHESIS YIELD (a.u.)
(111)
(100)
(110)
XBL 839-6407

Fig. 5

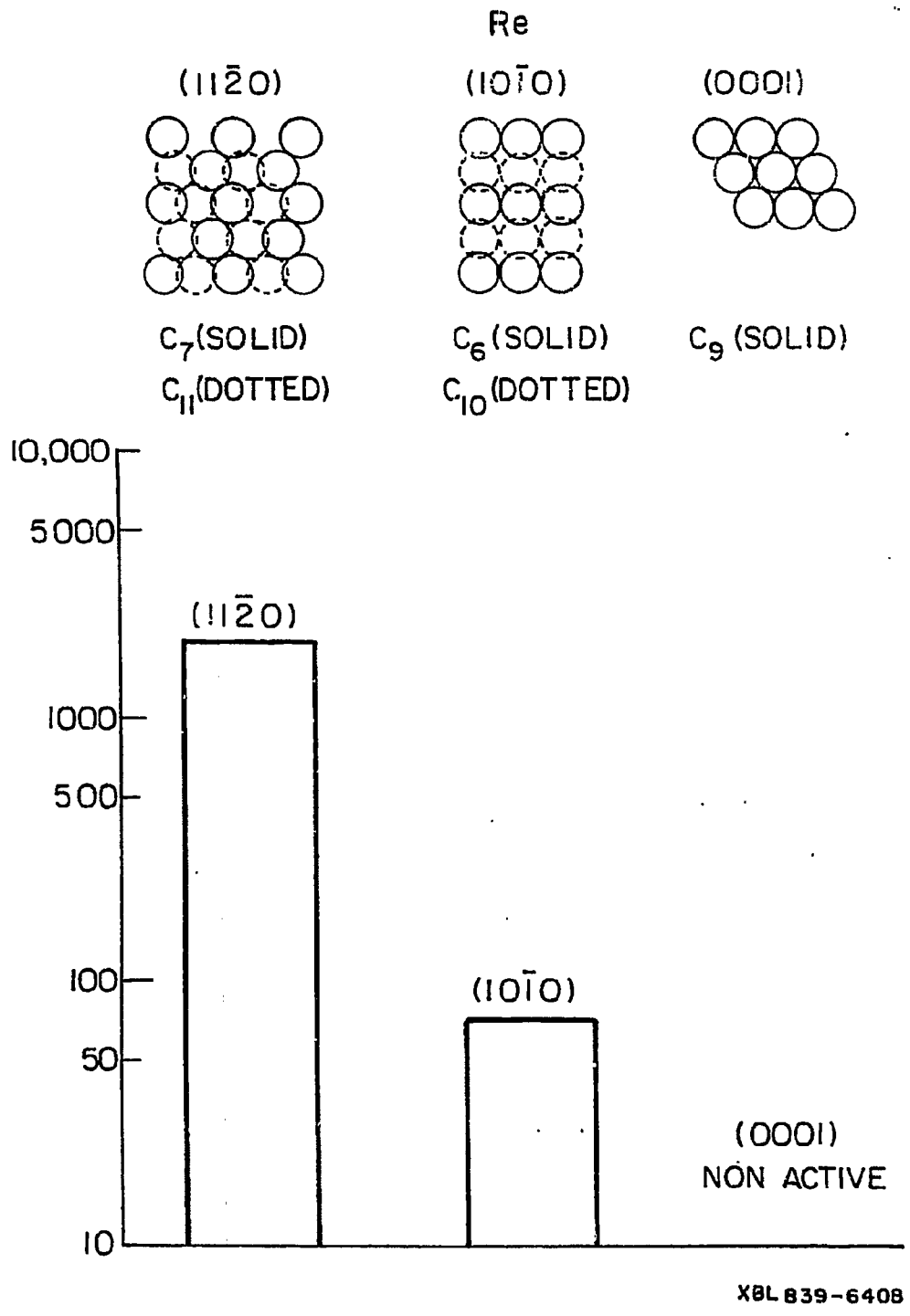
Re
(11$\bar{2}$0)
(10$\bar{1}$0)
(0001)
C_7(SOLID)
C_{11}(DOTTED)
C_6(SOLID)
C_{10}(DOTTED)
C_9 (SOLID)
10,000
5000
1000
500
100
50
10
(11$\bar{2}$0)
(10$\bar{1}$0)
(0001)
NON ACTIVE
XBL 839-6408

Fig. 6

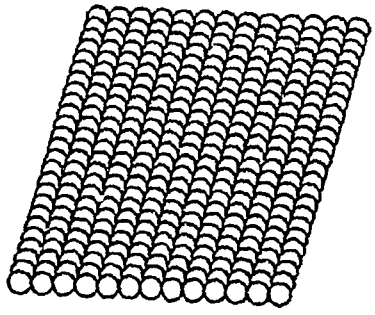

fcc (100)

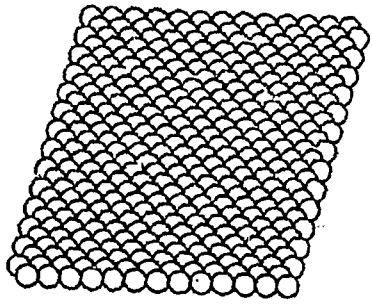

fcc (111)

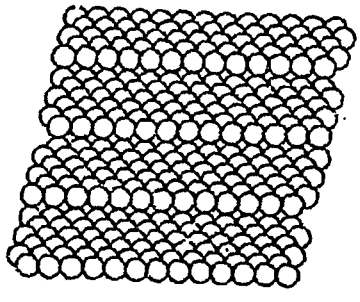

fcc (755)

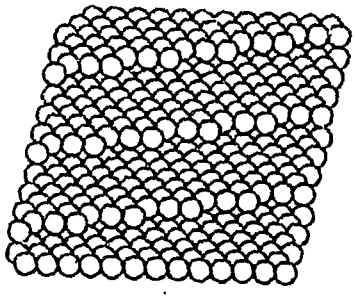

fcc (10.8.7)

XBL 8112-13009

Fig. 7

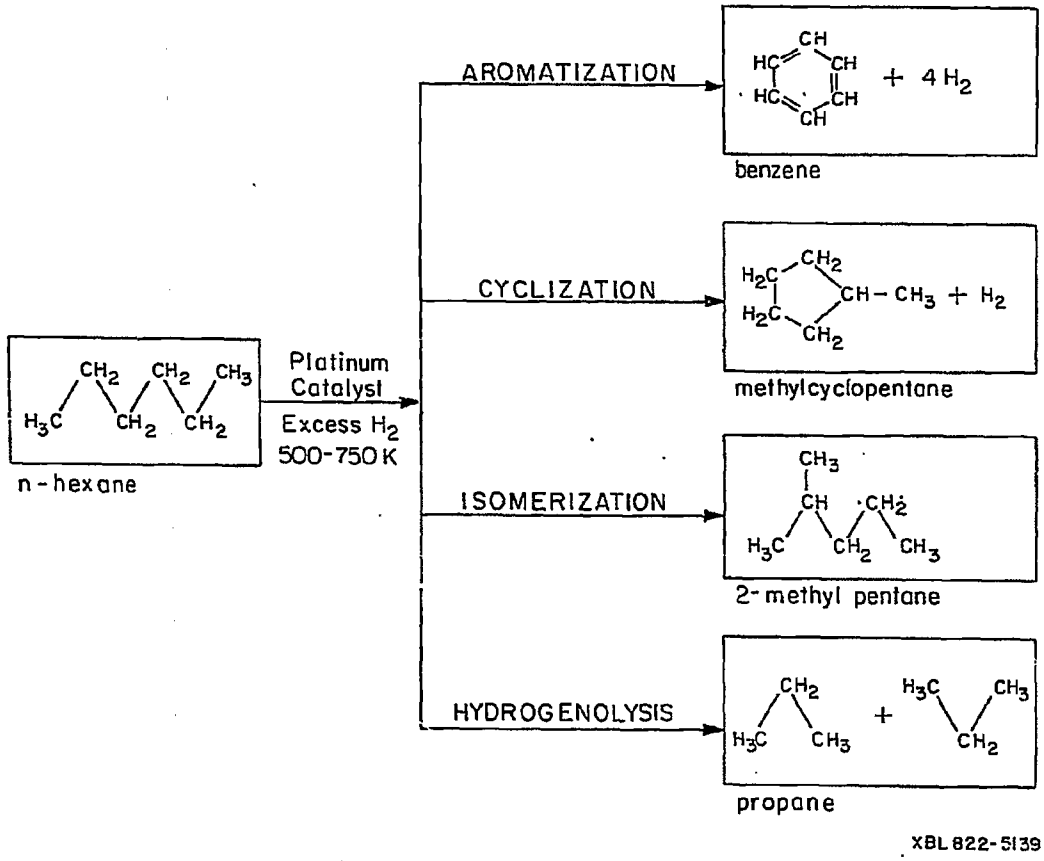
AROMATIZATION
+ 4 H2
benzene
CYCLIZATION
+ H2
methylcyclopentane
Platinum
Catalyst
Excess H2
500-750 K
n-hexane
ISOMERIZATION
2-methyl pentane
HYDROGENOLYSIS
+
propane
XBL 822-5139

Fig. 8

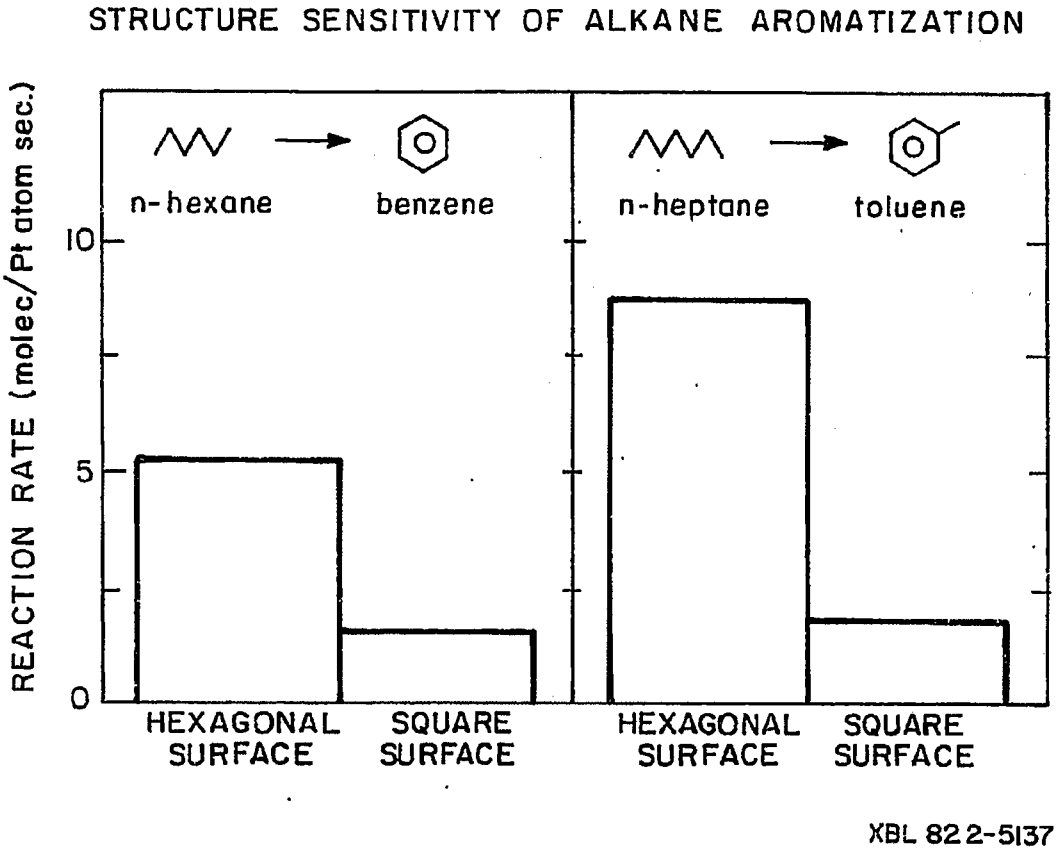
STRUCTURE SENSITIVITY OF ALKANE AROMATIZATION
REACTION RATE (molec/Pt atom sec.)
10
5
0
n-hexane
benzene
n-heptane
toluene
HEXAGONAL SURFACE
SQUARE SURFACE
HEXAGONAL SURFACE
SQUARE SURFACE
XBL 822-5137

Fig. 9

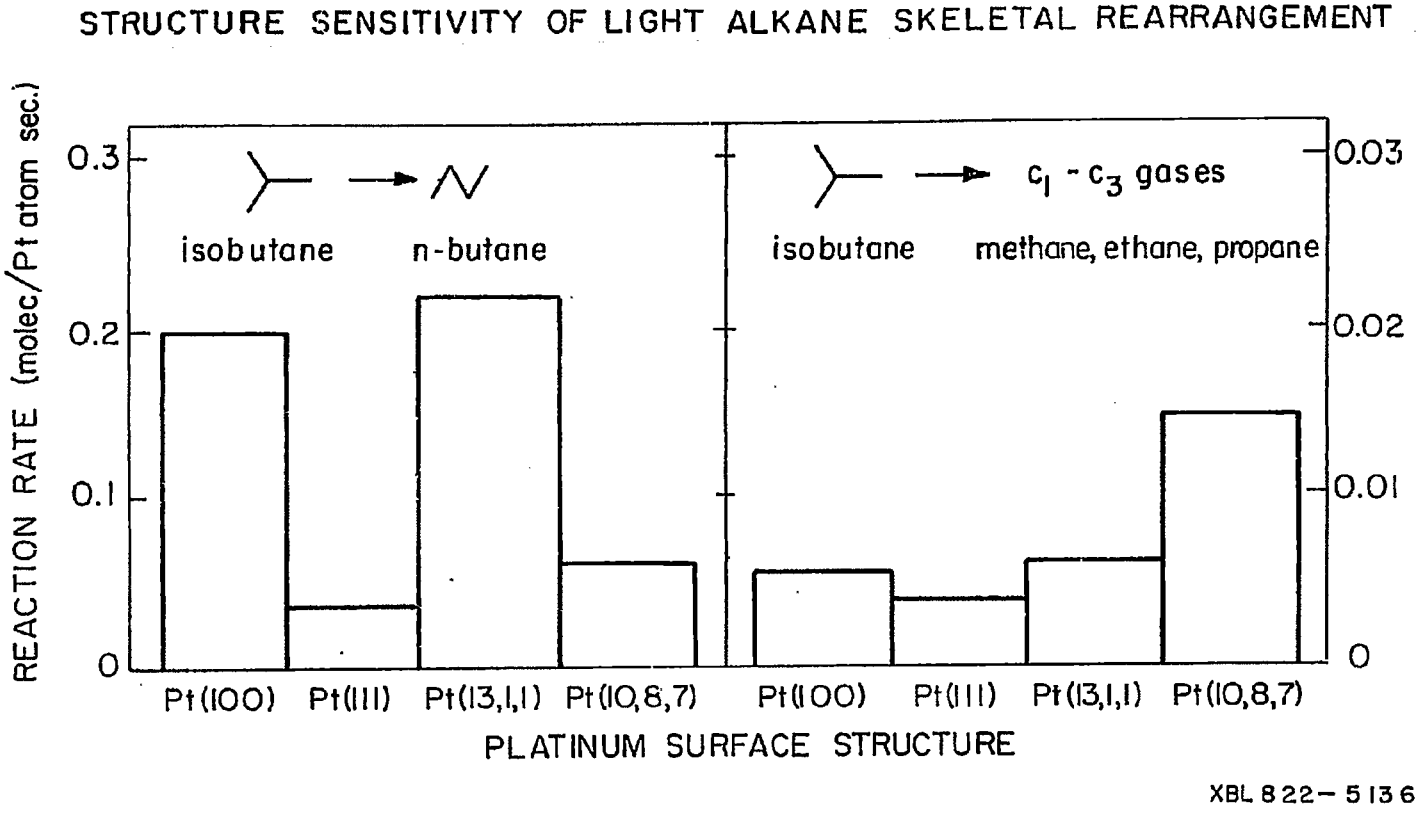
STRUCTURE SENSITIVITY OF LIGHT ALKANE SKELETAL REARRANGEMENT
REACTION RATE (molec/Pt atom sec.)
0.3
0.2
0.1
0
isobutane
n-butane
isobutane
$C_1 - C_3$ gases
methane, ethane, propane
0.03
0.02
0.01
0
Pt(100)
Pt(111)
Pt(13,1,1)
Pt(10,8,7)
Pt(100)
Pt(111)
Pt(13,1,1)
Pt(10,8,7)
PLATINUM SURFACE STRUCTURE
XBL 822-5136

Fig. 10

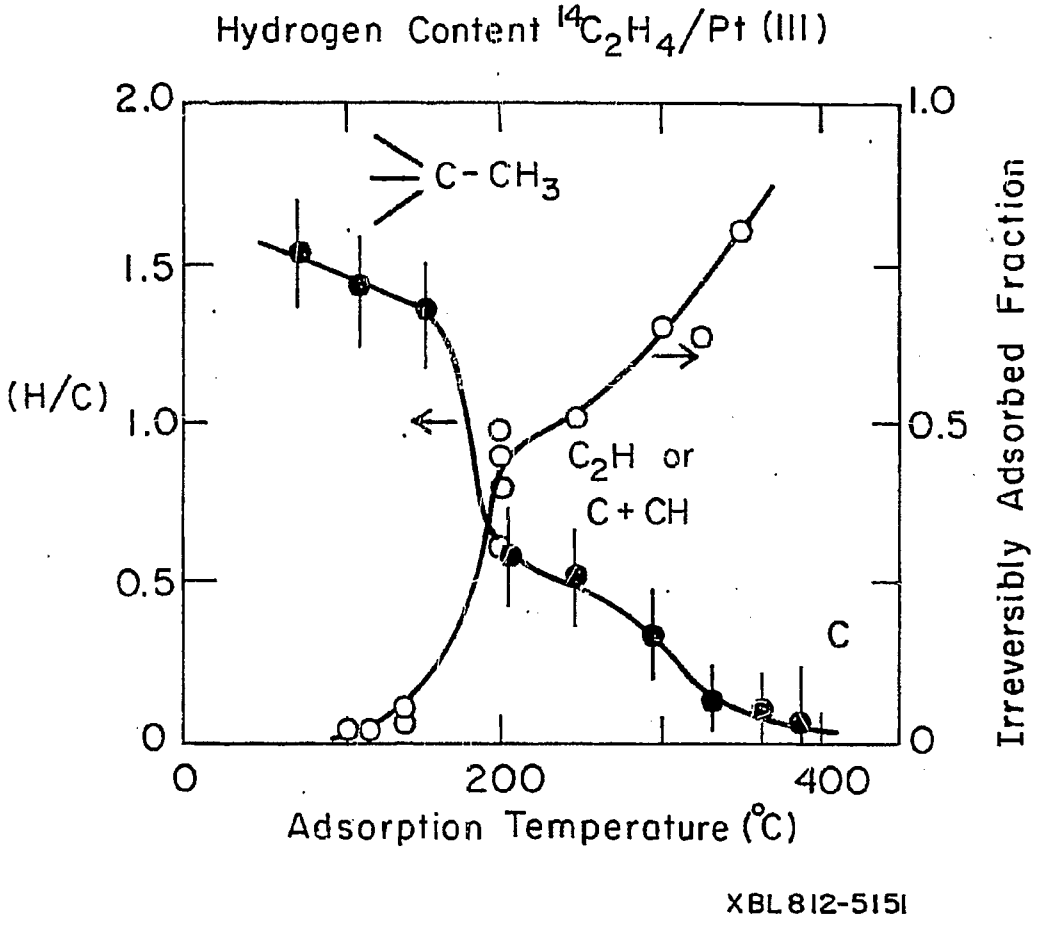
Hydrogen Content $^{14}C_2H_4$/Pt (111)
2.0
1.5
1.0
0.5
0
(H/C)
1.0
0.5
0
Irreversibly Adsorbed Fraction
C-CH3
C2H or
C + CH
C
0
200
400
Adsorption Temperature (°C)
XBL812-5151

Fig. 11

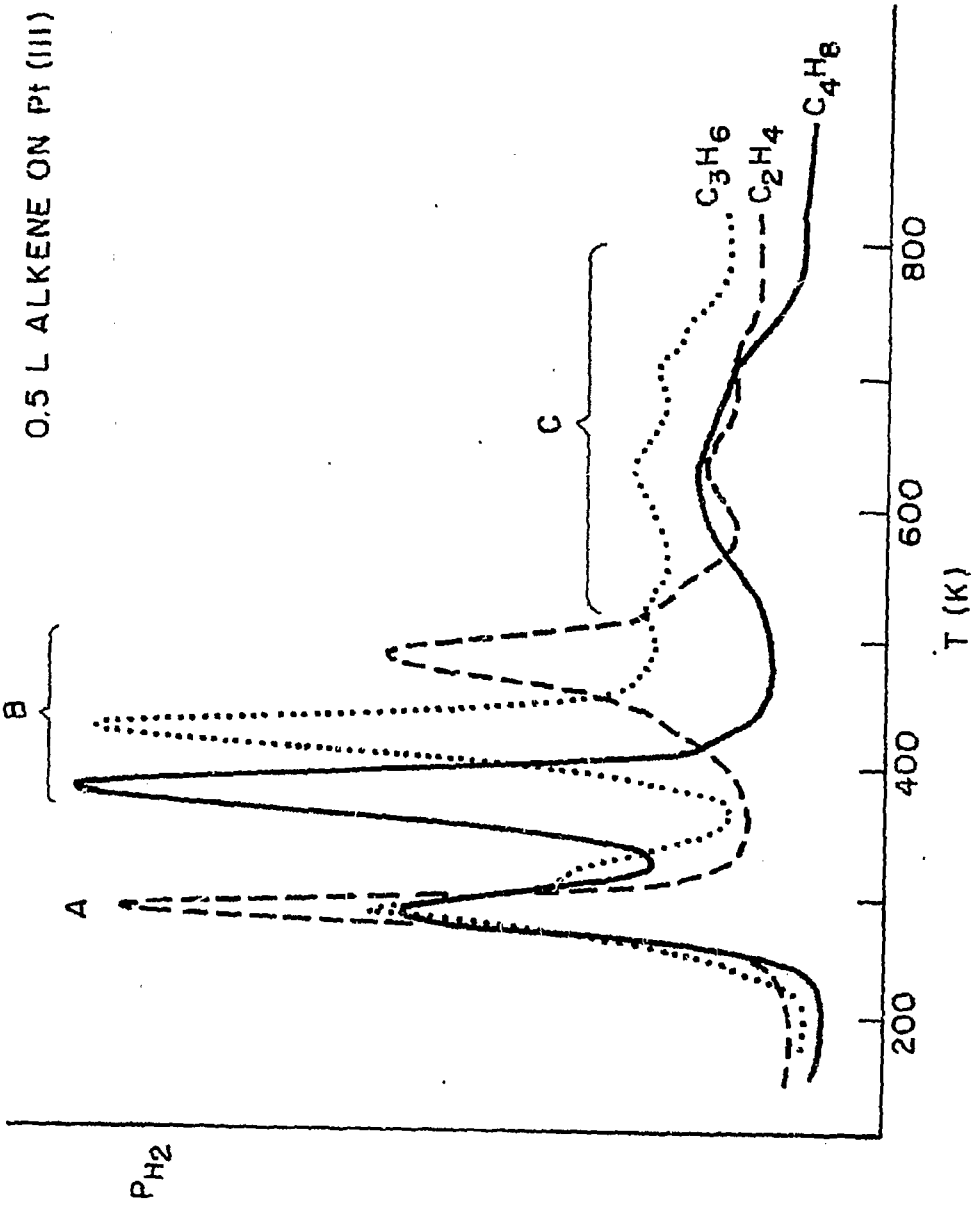
0.5 L ALKENE ON Pt (111)
A
B
C
C_3H_6
C_2H_4
C_4H_8
P_{H2}
200
400
600
800
T (K)
XBL 814-5475

Fig. 12

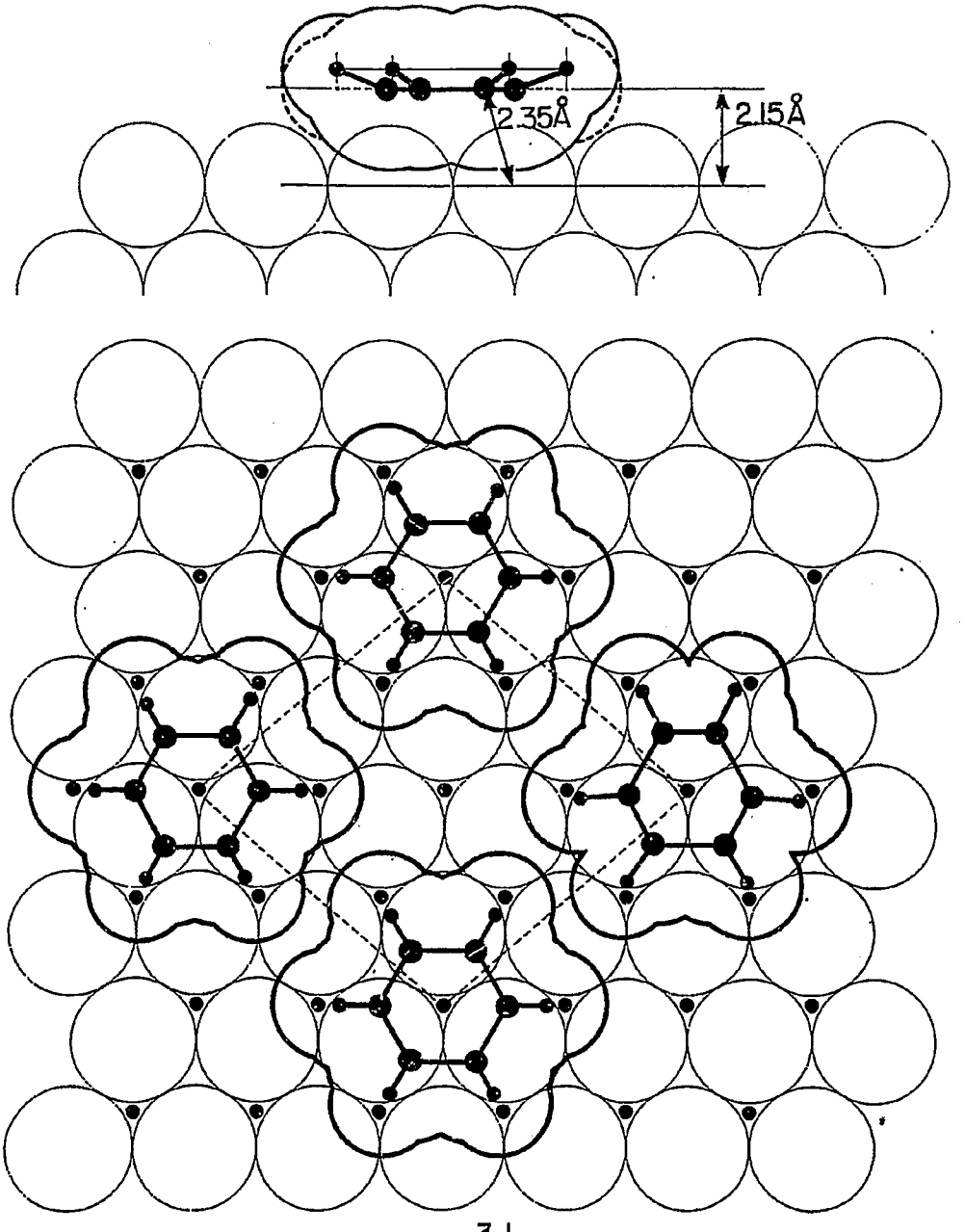

$Rh(111)-\begin{pmatrix} 3 & 1 \\ 1 & 3 \end{pmatrix} C_6H_6$

XBL 835-198

Fig. 13

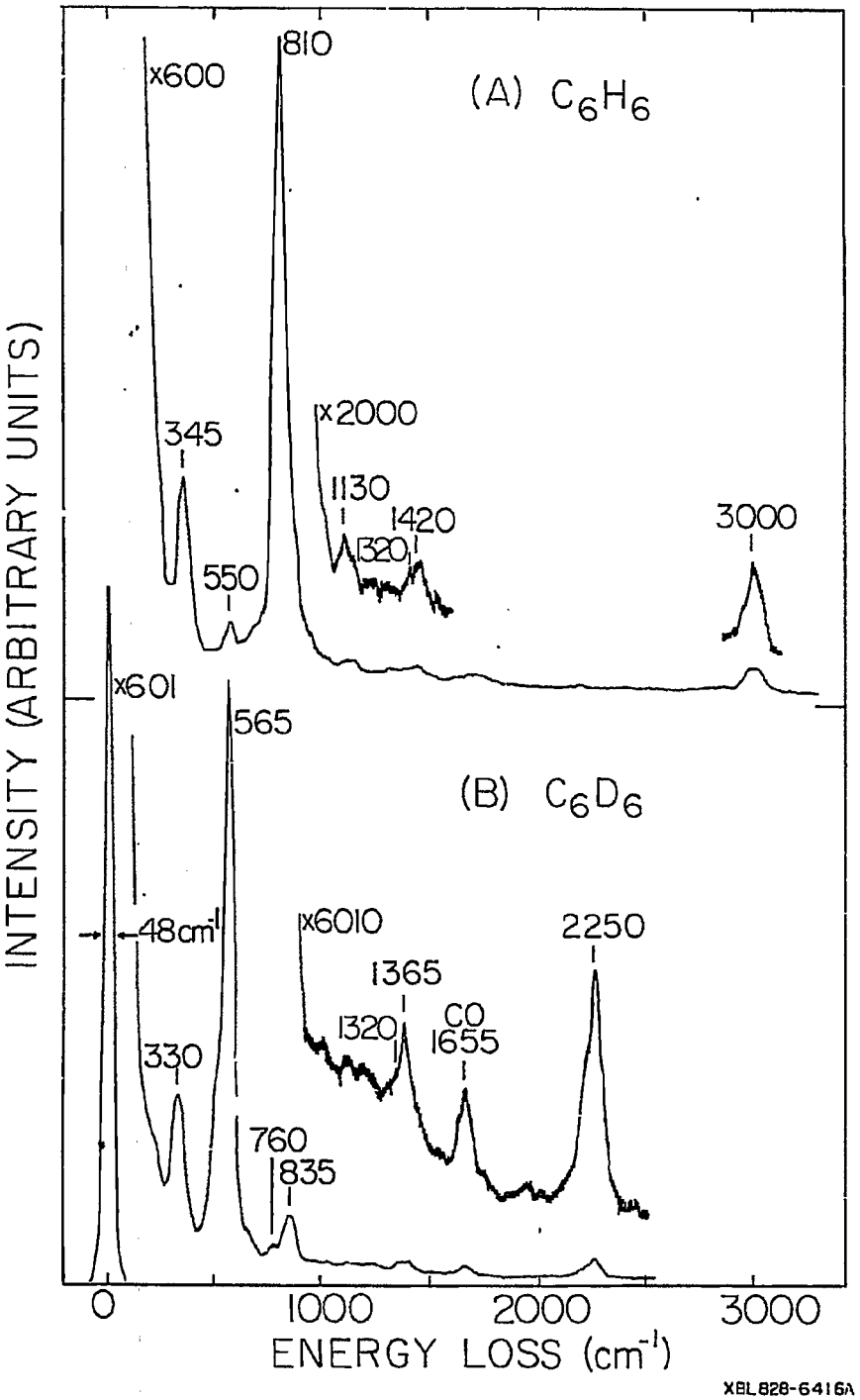
INTENSITY (ARBITRARY UNITS)
x600
810
(A) C_6H_6
x2000
345
1130
1420
1320
550
3000
x601
565
(B) C_6D_6
48cm⁻¹
x6010
2250
1365
1320
CO
1655
330
760
835
0
1000
2000
3000
ENERGY LOSS (cm⁻¹)
XBL828-6416A

Fig. 14

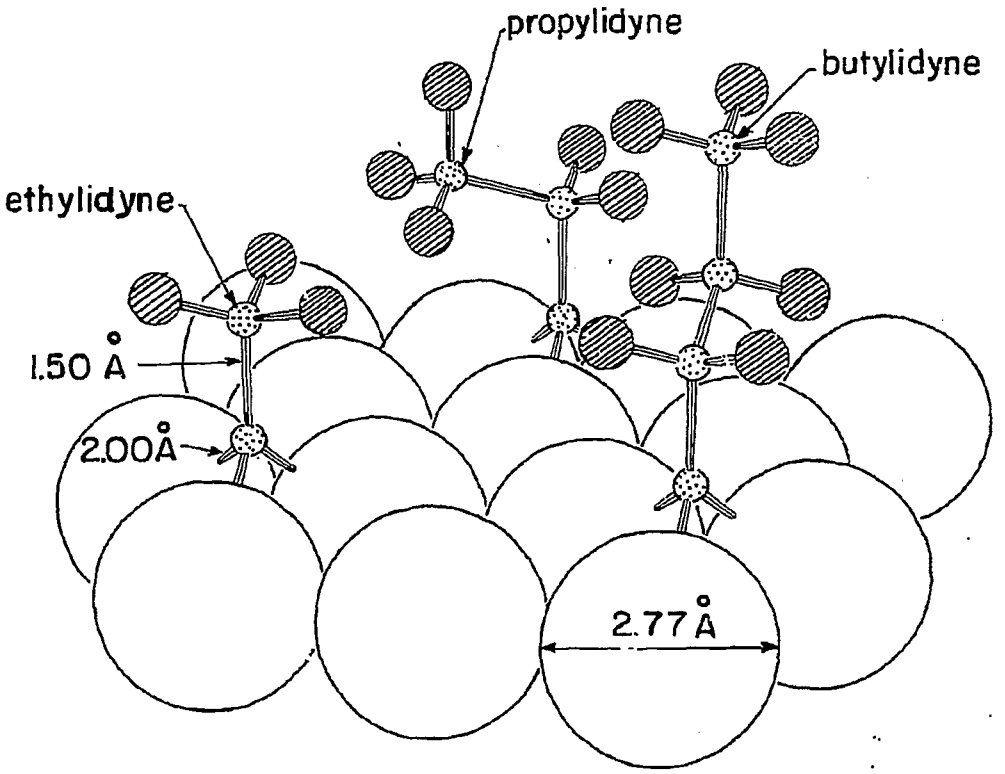

Pt(111) + ethylidyne, propylidyne and butylidyne

XBL 8110-6882

Fig. 15

Different ethylidyne species: bond distances and angles
(r_C = carbon covalent radius; r_M = bulk metal atomic radius)

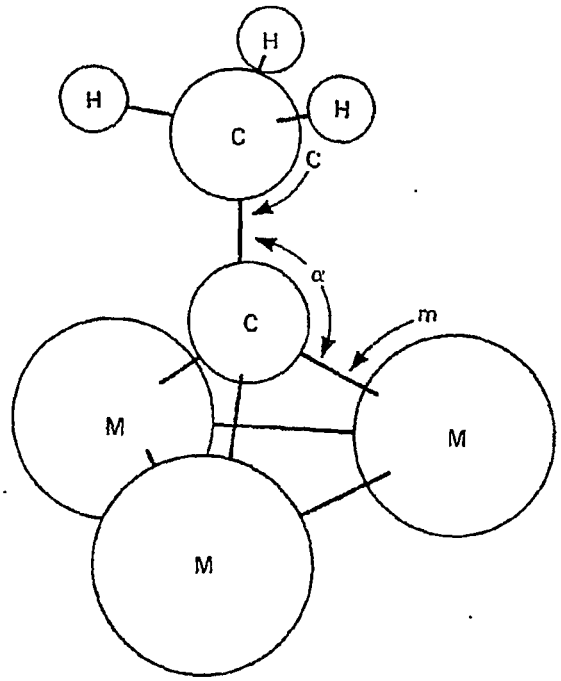

	C [Å]	m	r_M	r_C	α [°]
$Co_3 (CO)_9 CCH_3$	1.53 (3)	1.90 (2)	1.25	0.65	131.3
$H_3 Ru_3 (CO)_9 CCH_3$	1.51 (2)	2.08 (1)	1.34	0.74	128.1
$H_3 Os_3 (CO)_9 CCH_3$	1.51 (2)	2.08 (1)	1.35	0.73	128.1
Pt (111) + (2 X 2) CCH_3	1.50	2.00	1.39	0.61	127.0
Rh (111) + (2 X 2) CCH_3	1.45 (10)	2.03 (7)	1.34	0.69	130.2
$H_3C - CH_3$	1.54			0.77	109.5
$H_2C = CH_2$	1.33			0.68	122.3
$HC \equiv CH$	1.20			0.60	180.0

XBL 818-11196

Fig. 16

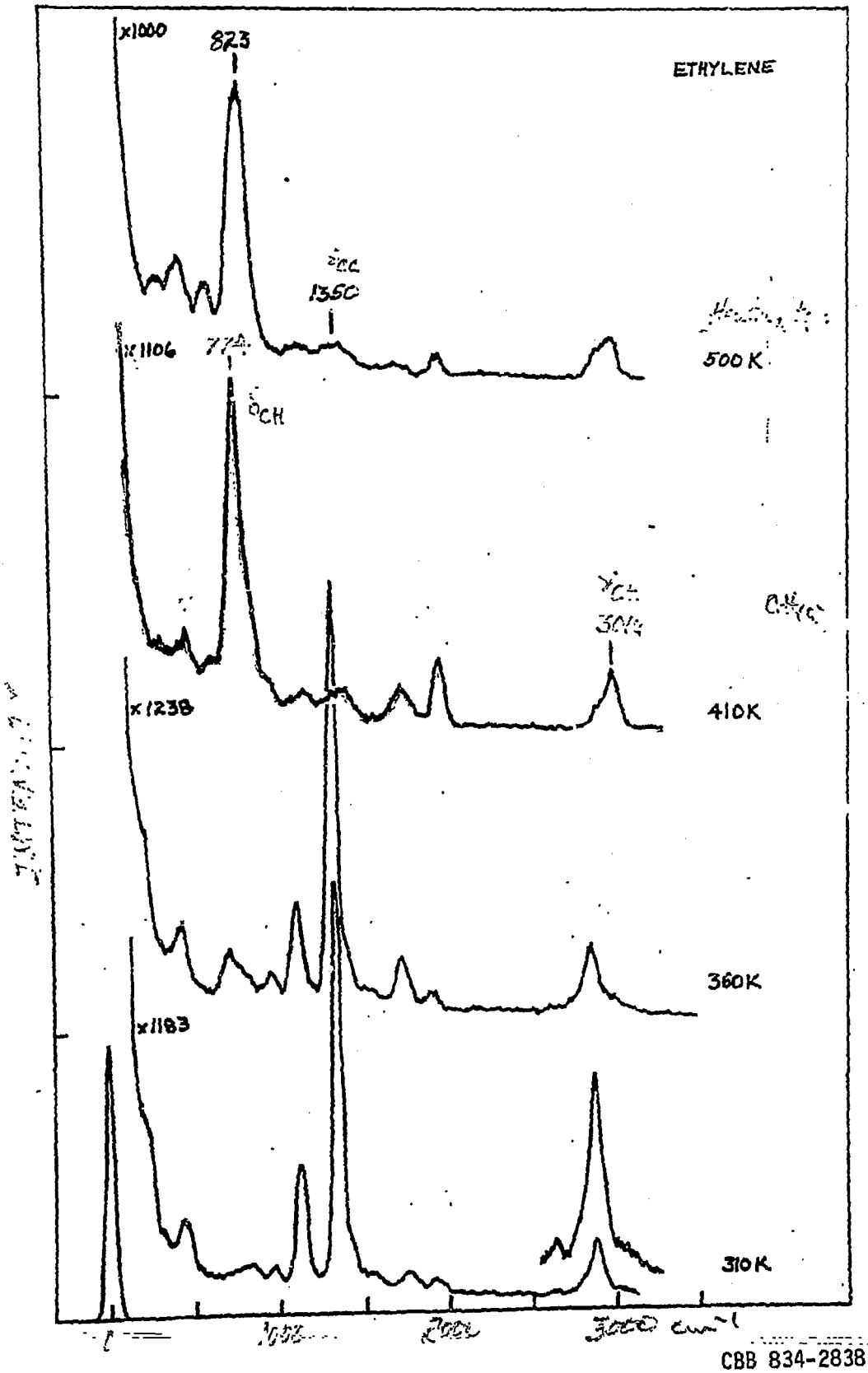
ETHYLENE
x1000
823
1350
500 K
x1106
774
410K
x1238
360K
x1183
310K
3000 cm⁻¹
CBB 834-2838

Fig. 17

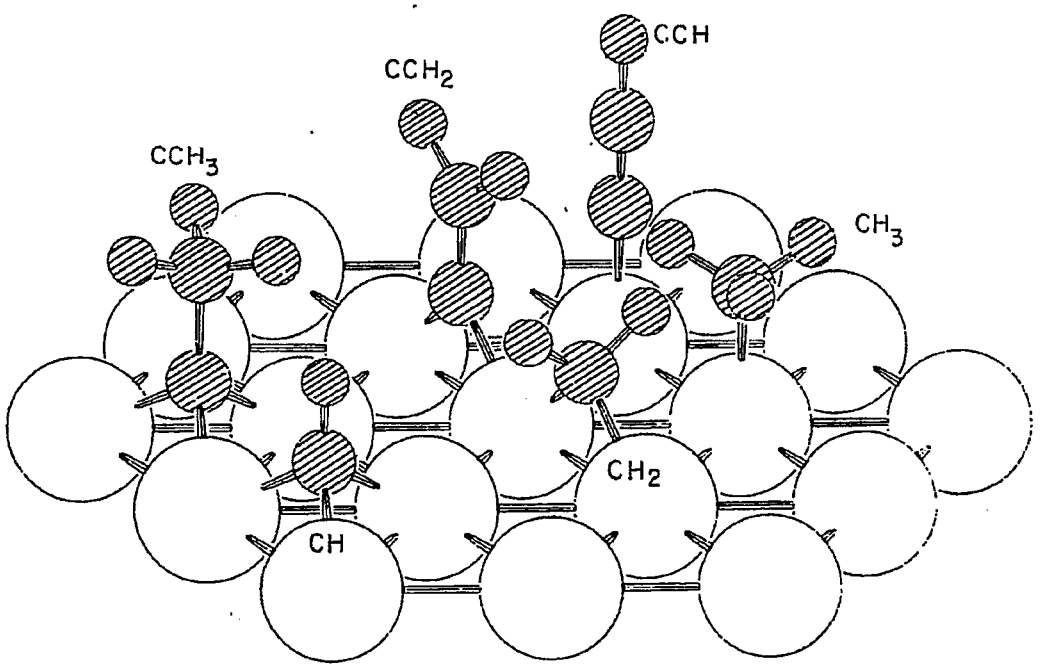

XBL 826-5941

Fig. 18

CO Chemisorption on Carbon Covered Pt(111), Pt(100) and Pt(13, 1,1)

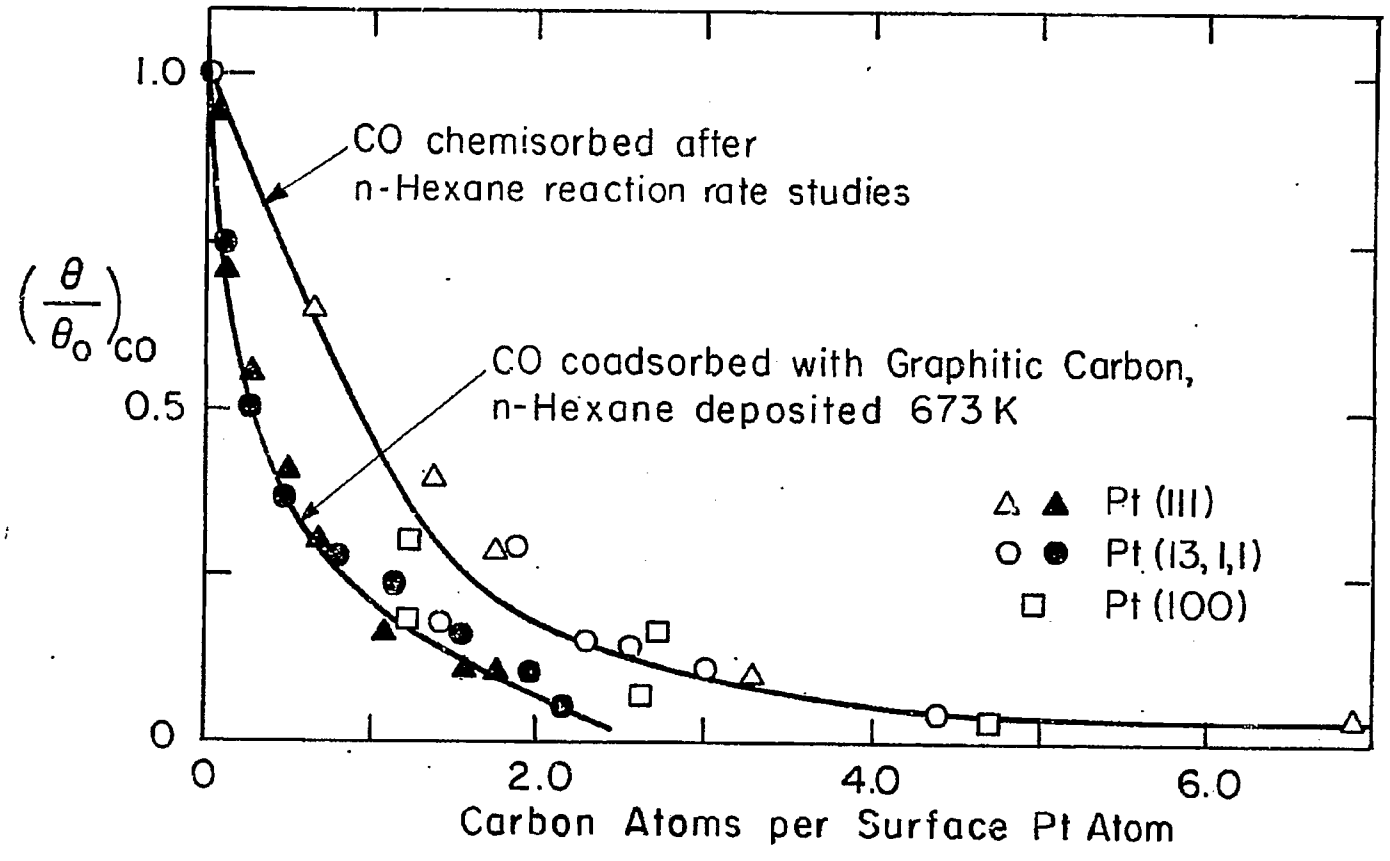

XBL 816-5851

Fig. 19

MODEL FOR THE WORKING PLATINUM CATALYST

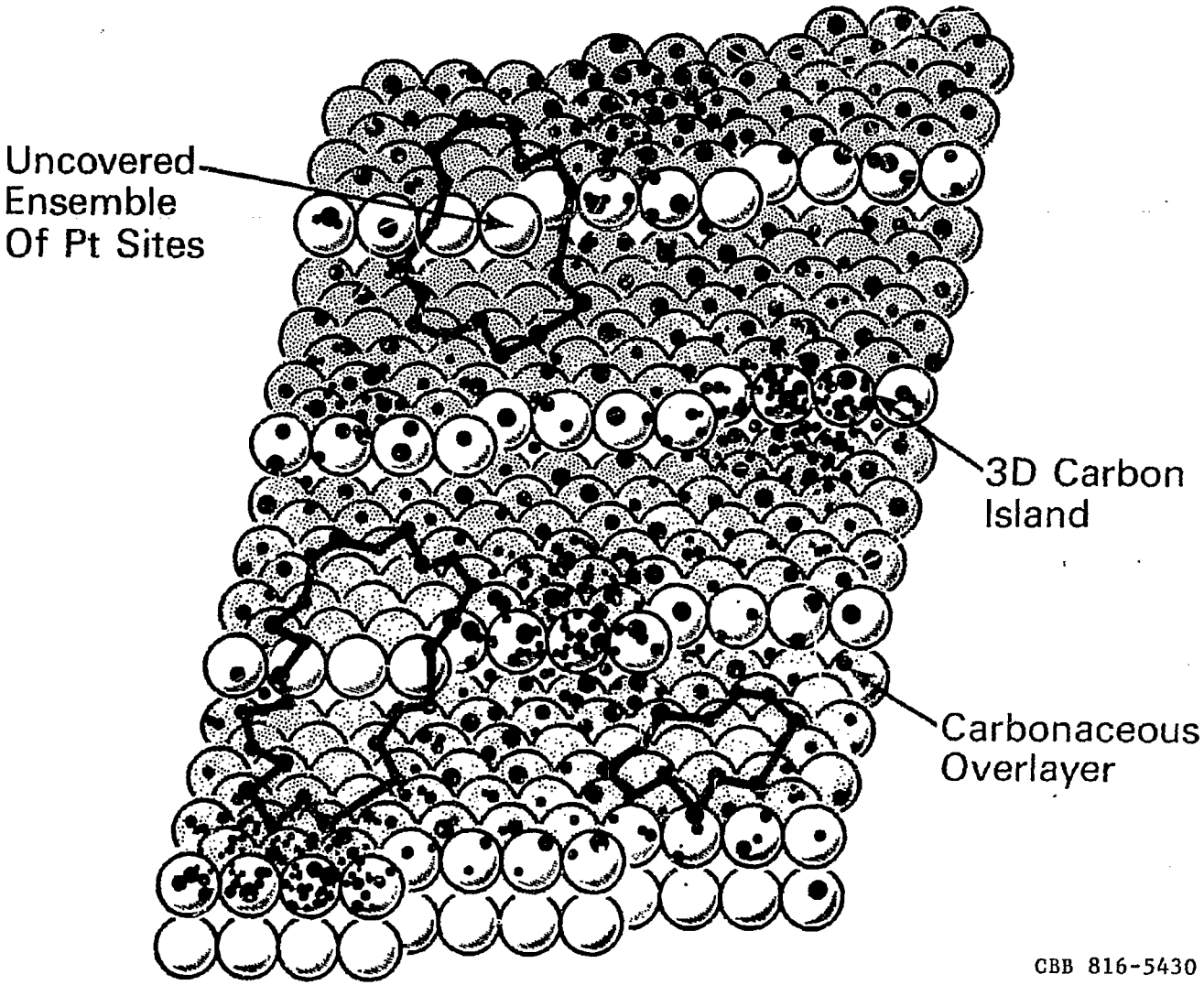

Fig. 20

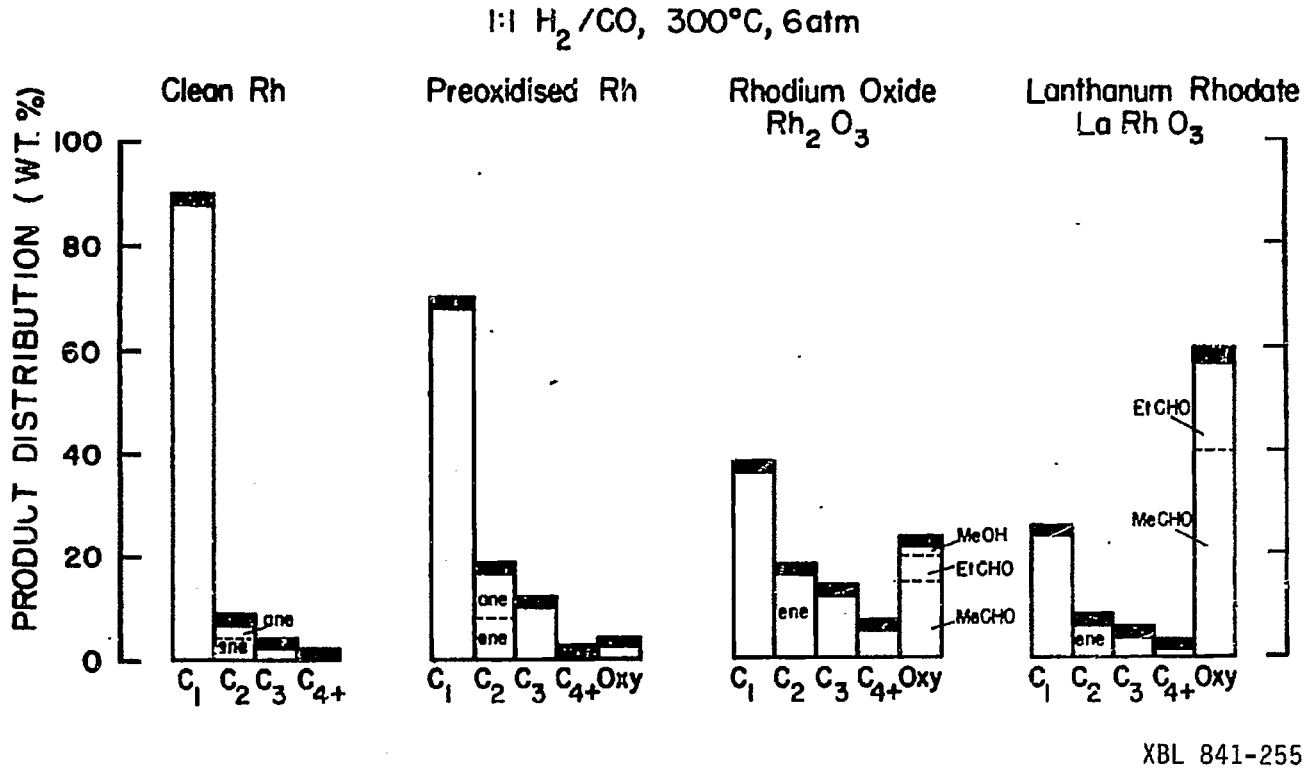
1:1 H2/CO, 300°C, 6atm
Clean Rh
Preoxidised Rh
Rhodium Oxide
Rh2 O3
Lanthanum Rhodate
La Rh O3
PRODUCT DISTRIBUTION (WT.%)
100
80
60
40
20
0
ane
ene
MeOH
EtCHO
MeCHO
C1 C2 C3 C4+ Oxy
XBL 841-255

Fig. 21

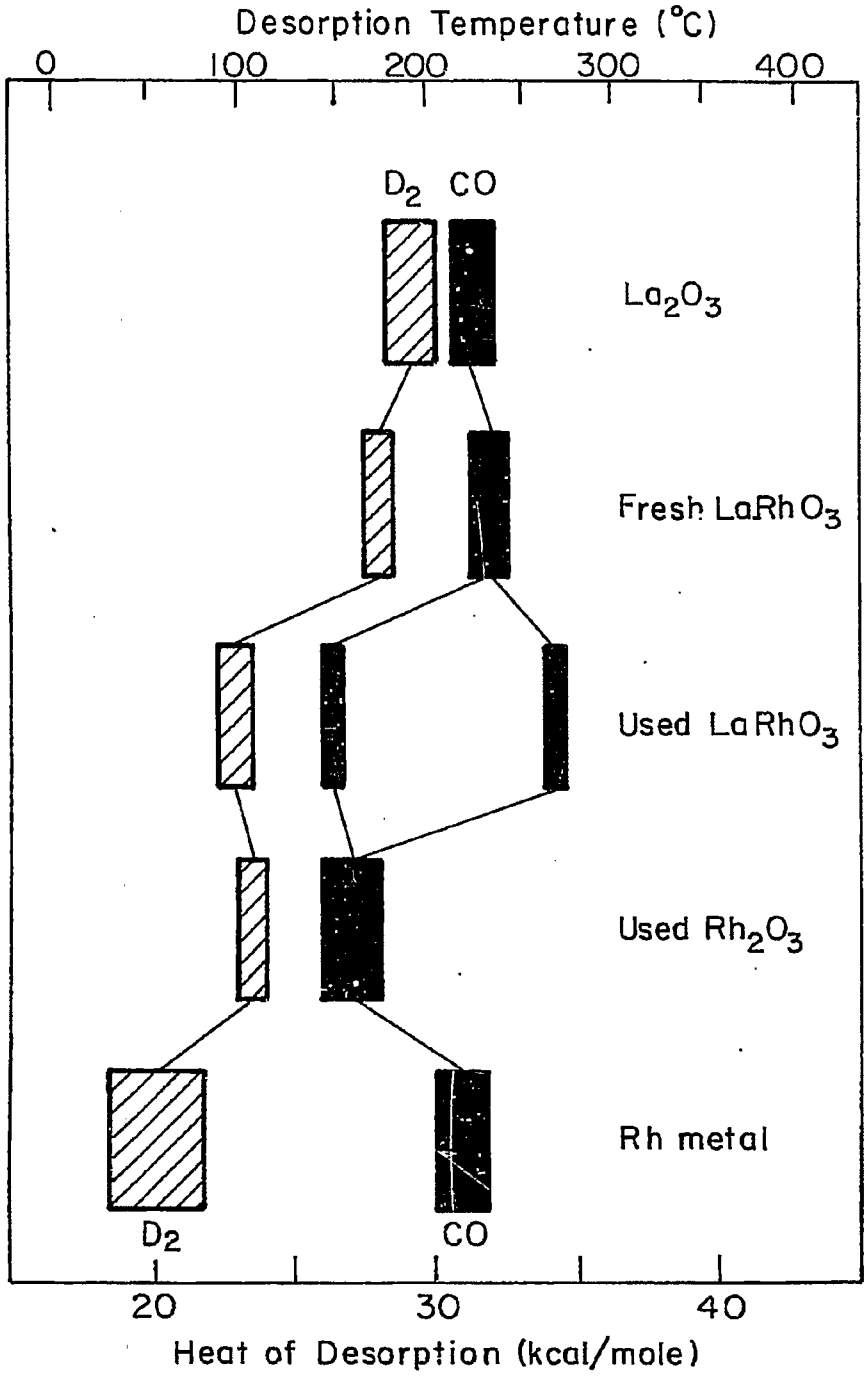

XBL 817-6123

Fig. 22

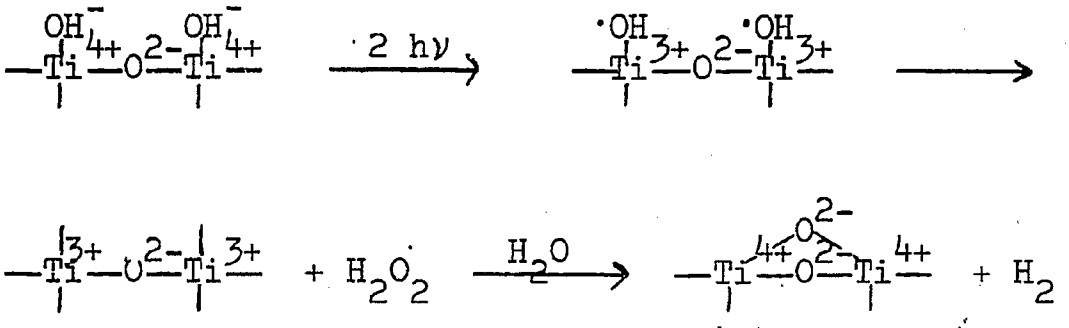

Van Damme and Hall, JACS 101 4373

XBL 822-7816

Fig. 23

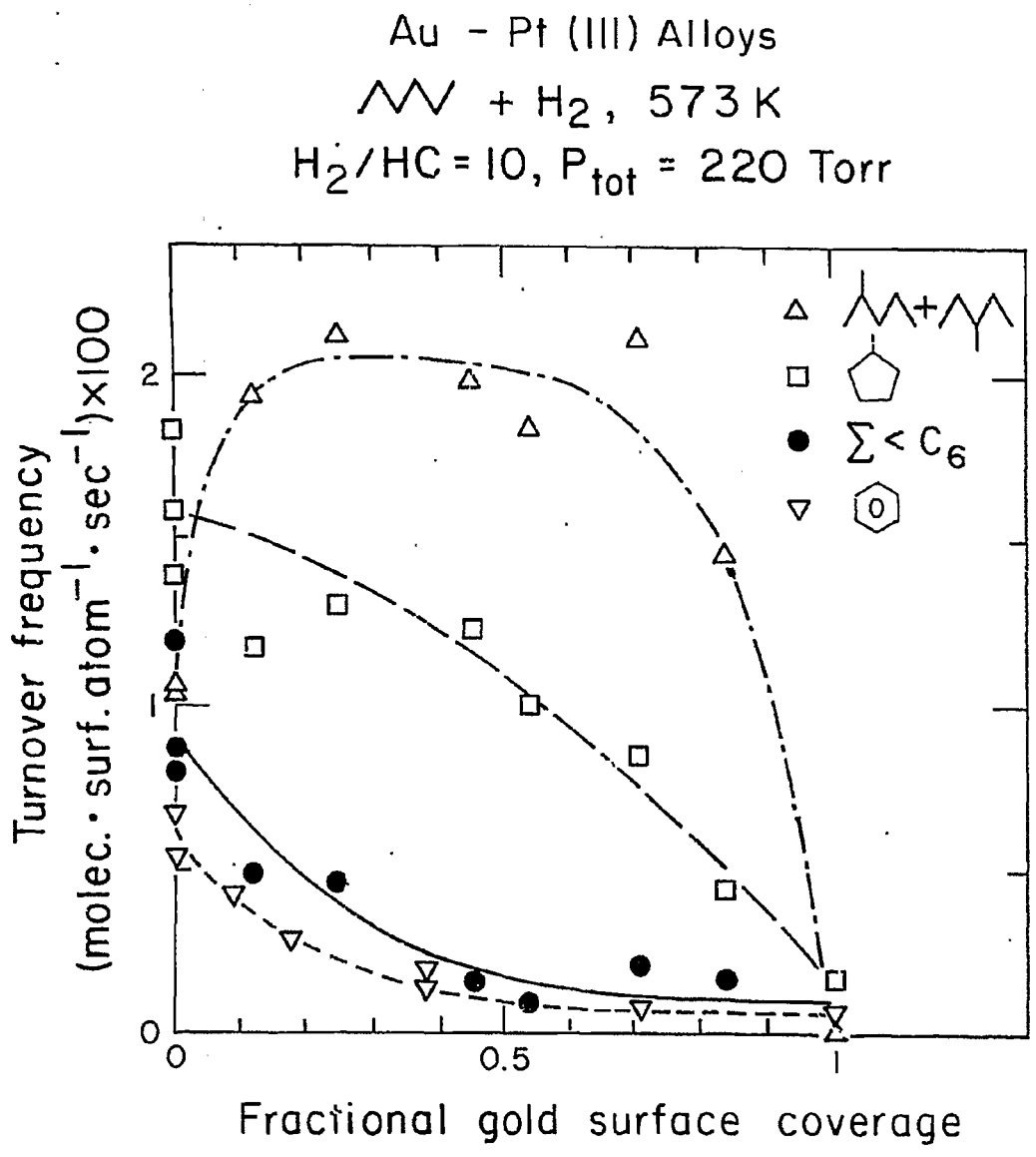

XBL 819-2495

Fig. 24

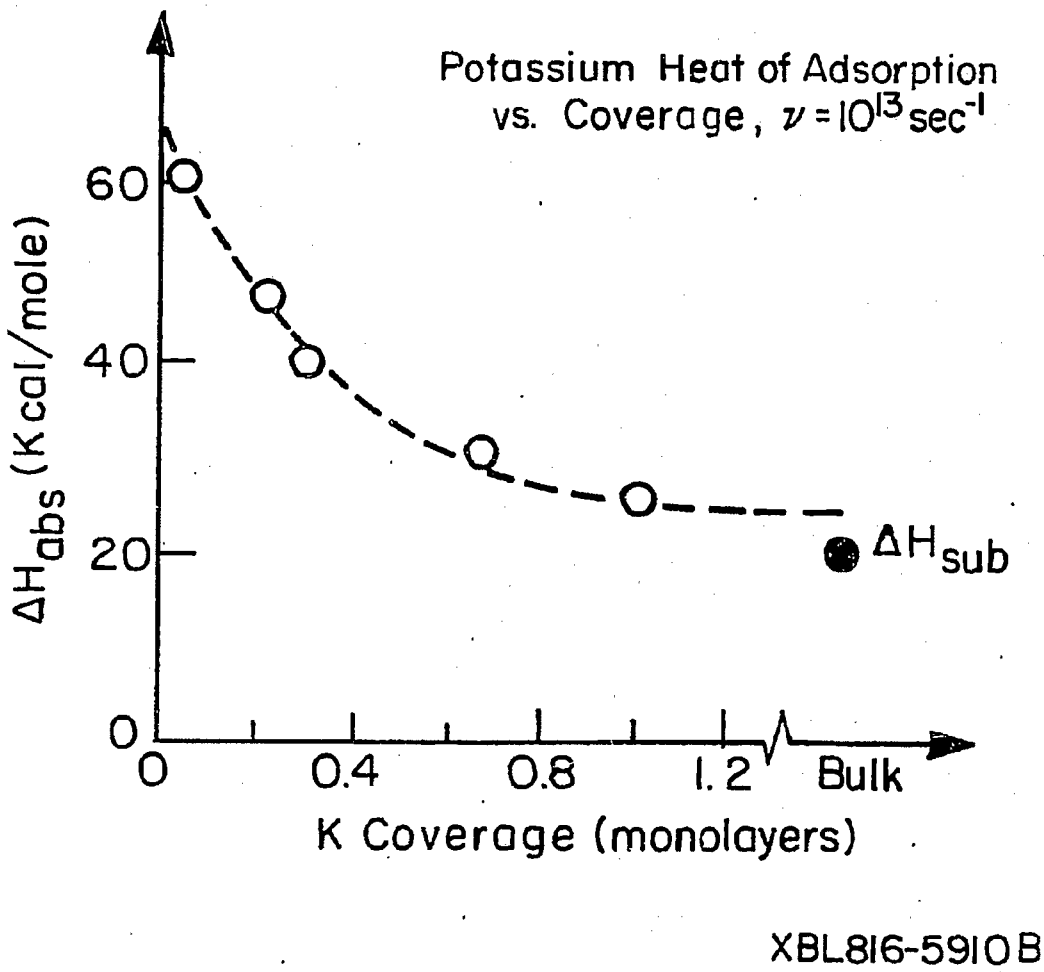

XBL816-5910B

Fig. 25

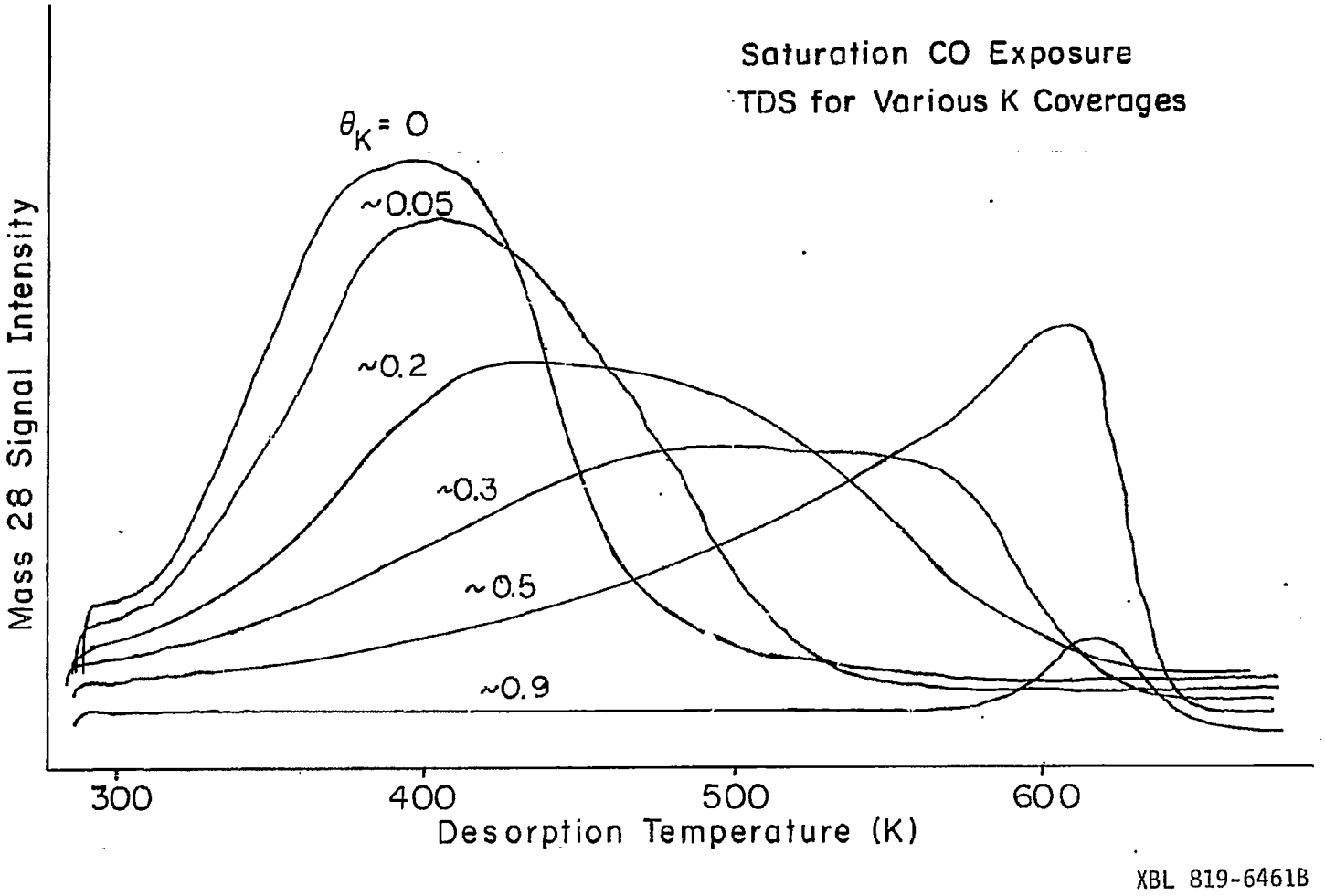

XBL 819-6461B

Fig. 26

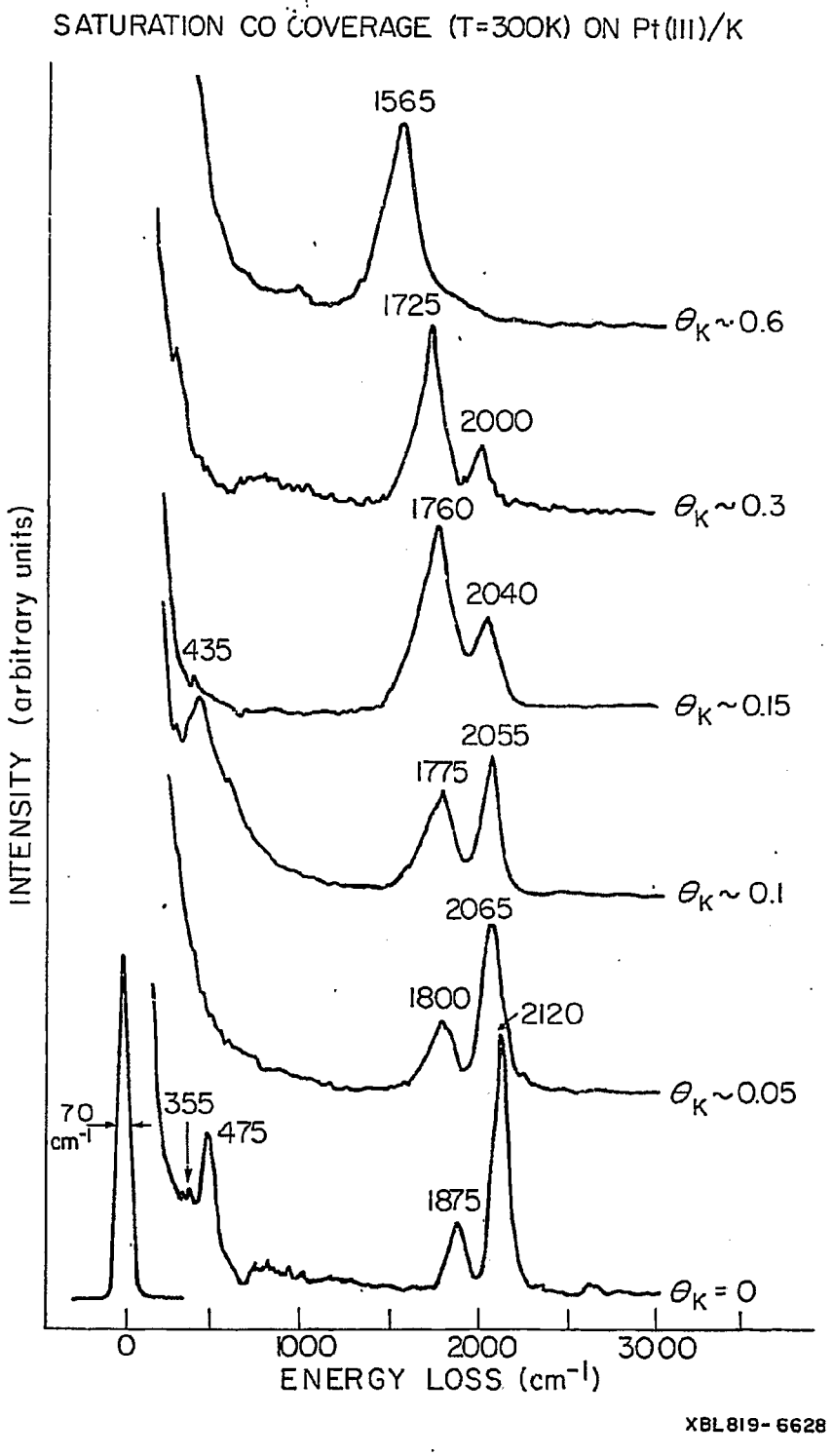
SATURATION CO COVERAGE (T=300K) ON Pt(111)/K
1565
1725
θ_K~0.6
2000
1760
θ_K~0.3
2040
435
θ_K~0.15
2055
1775
θ_K~0.1
2065
1800
2120
θ_K~0.05
70 cm^{-1}
355
475
1875
θ_K = 0
INTENSITY (arbitrary units)
0
1000
2000
3000
ENERGY LOSS (cm^{-1})
XBL819-6628

Fig. 27

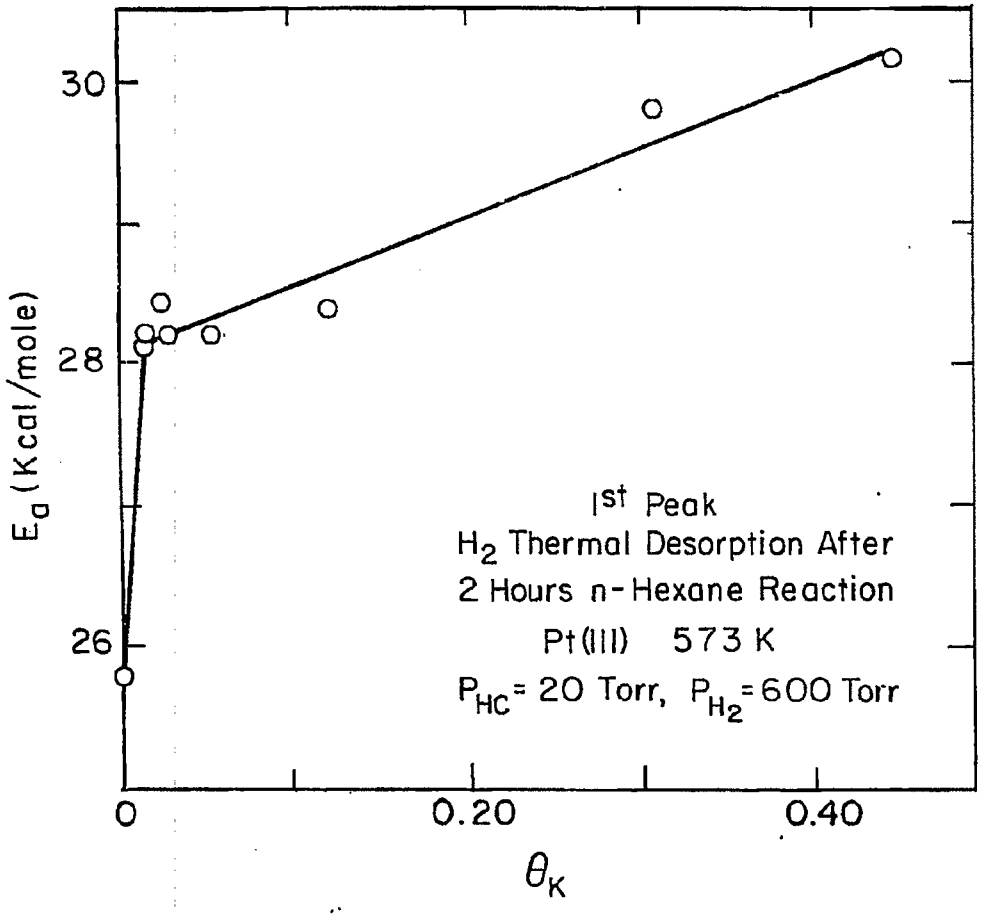
30
28
26
E_a (Kcal/mole)
0
0.20
0.40
θ_K
1st Peak
H_2 Thermal Desorption After
2 Hours n-Hexane Reaction
Pt(111) 573 K
P_{HC} = 20 Torr, P_{H_2} = 600 Torr
XBL 823-5304 A

Fig. 28

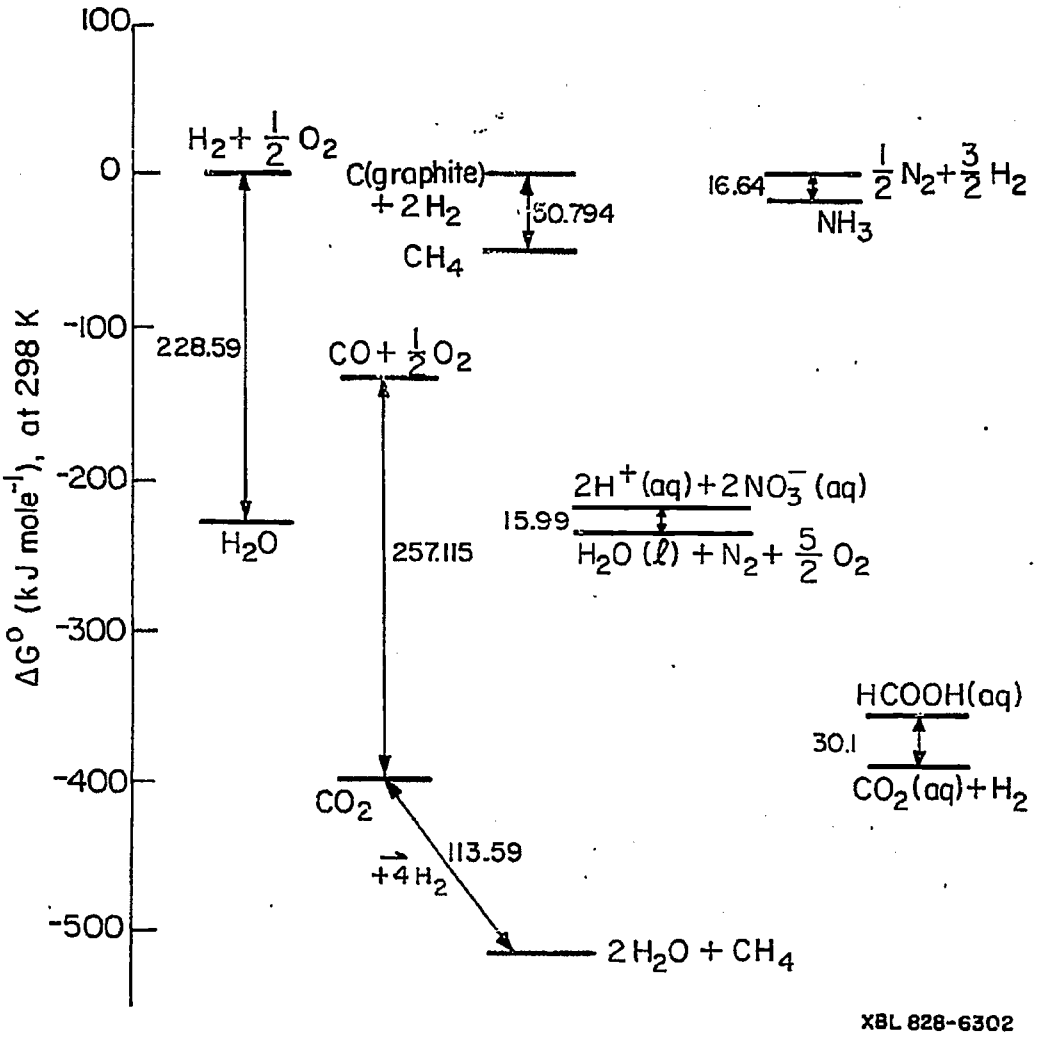
100
0
-100
-200
-300
-400
-500
ΔG° (kJ mole⁻¹), at 298 K
H2 + 1/2 O2
228.59
H2O
C(graphite) + 2 H2
50.794
CH4
CO + 1/2 O2
257.115
CO2
+4 H2
113.59
2 H2O + CH4
16.64
1/2 N2 + 3/2 H2
NH3
2H+(aq) + 2NO3−(aq)
15.99
H2O (ℓ) + N2 + 5/2 O2
HCOOH(aq)
30.1
CO2(aq) + H2
XBL 828-6302

Fig. 29(a)

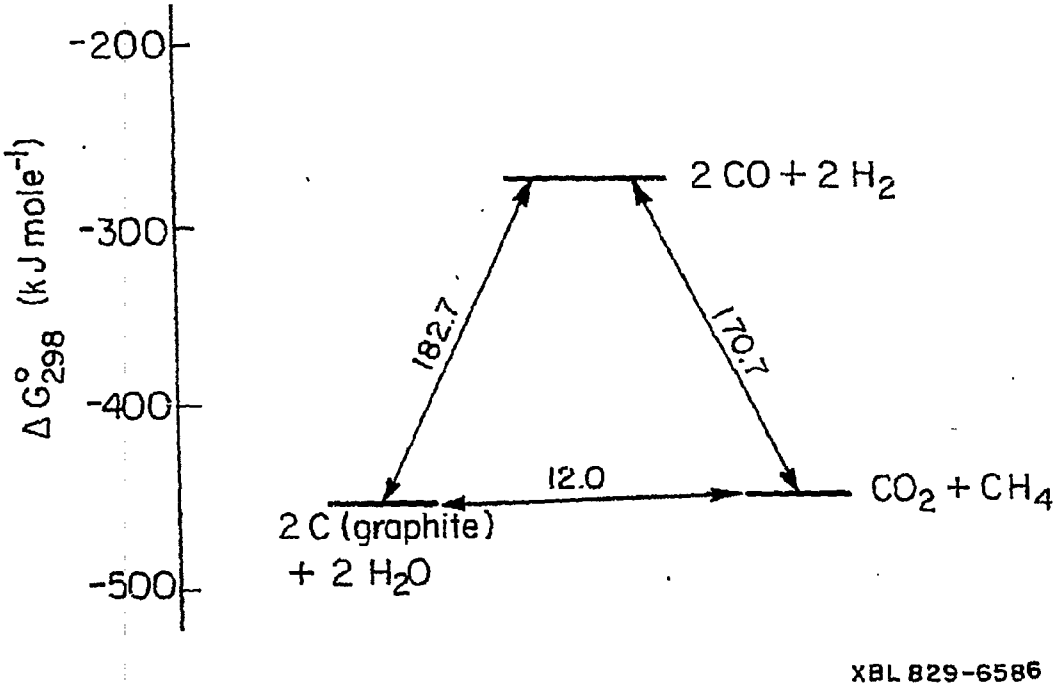
-200
-300
-400
-500
ΔG°_{298} (kJ mole^{-1})
2 CO + 2 H_2
182.7
170.7
12.0
CO_2 + CH_4
2 C (graphite)
+ 2 H_2O
XBL 829-6586

Fig. 29(b)

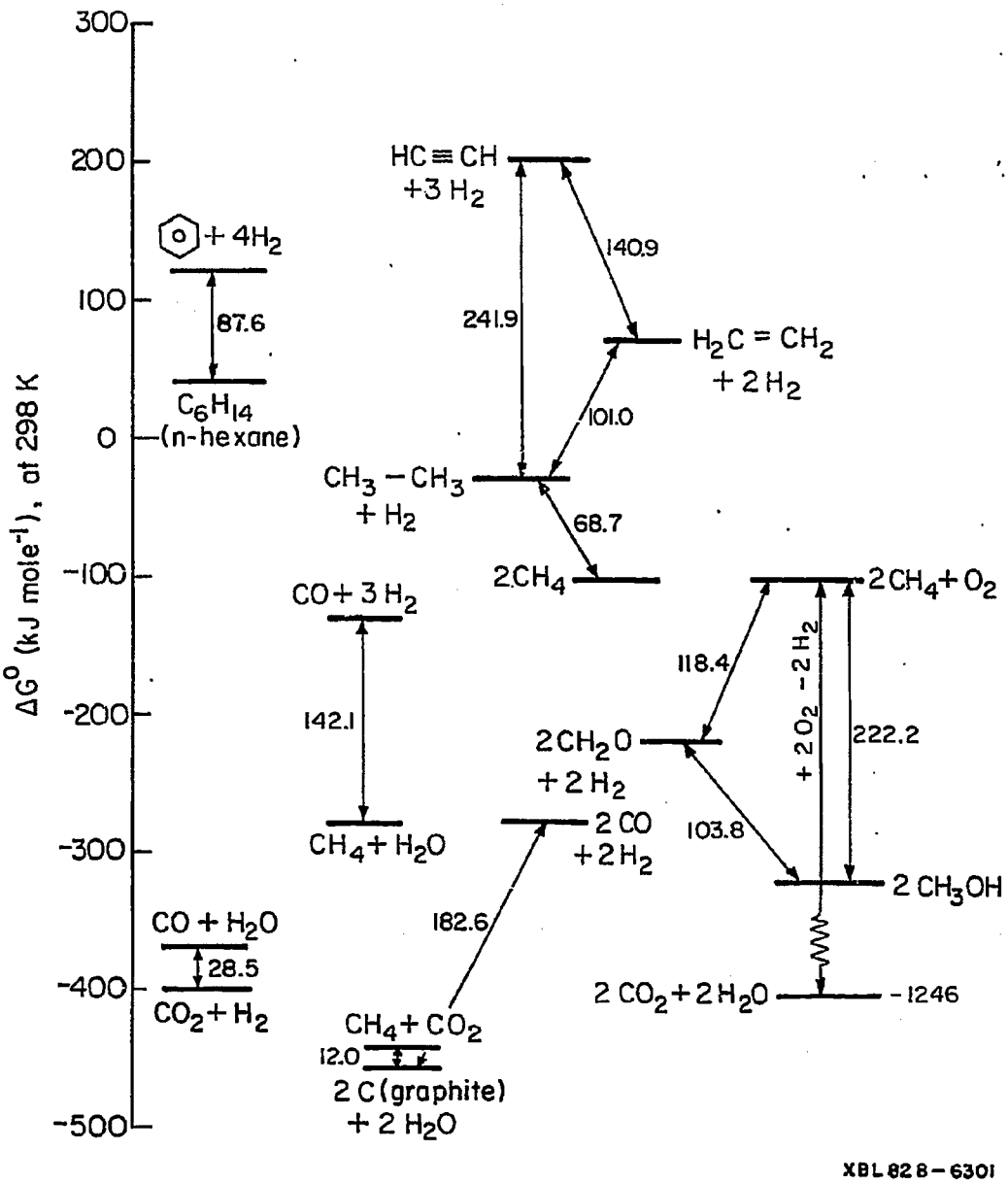
300
200
100
0
-100
-200
-300
-400
-500
ΔG° (kJ mole⁻¹), at 298 K
+ 4H2
87.6
C6H14
(n-hexane)
CO + H2O
28.5
CO2 + H2
HC≡CH
+3 H2
140.9
241.9
H2C = CH2
+ 2 H2
101.0
CH3 − CH3
+ H2
68.7
2CH4
CO + 3 H2
142.1
CH4 + H2O
2CH4 + O2
118.4
+ 2O2 − 2 H2
222.2
2CH2O
+ 2 H2
2 CO
+ 2 H2
103.8
2 CH3OH
182.6
2 CO2 + 2 H2O
-1246
CH4 + CO2
12.0
2 C (graphite)
+ 2 H2O
XBL 828-6301

Fig. 29(c)

U.S. DEPARTMENT OF COMMERCE
Technology Administration
National Technical Information Service
Springfield, VA 22161 (703) 605-6000